Limnol. Oceanogr., 53(5, part 2), 2008, 2062–2079

Air–sea CO_2 flux variability in frontal regions of the Southern Ocean from CARbon Interface OCean Atmosphere drifters

J. Boutin,[1] *L. Merlivat, C. Hénocq, and N. Martin*
LOCEAN, Laboratoire d'Océanographie et du Climat – Expérimentation et Approches Numériques/ Institut Pierre Simon Laplace, Unité Mixte de Recherche, CNRS/IRD/UPMC/MNHN, Paris, France

J. B. Sallée
LEGOS, Laboratoire d'Etudes en Géophysique et Océanographie Spatiale, Unité Mixte de Recherche CNRS/CNES/IRD/UPS, Toulouse, France

Abstract

Nine CARbon Interface OCean Atmosphere (CARIOCA) drifters were deployed in the Southern Ocean (south of the subtropical front, STF) between 2001 and 2006. They recorded 65 months of measurements in all seasons between 57°S and 40°S. Hydrological fronts detected by altimetry indicate that one buoy explored the polar zone (PZ) of the Atlantic Ocean and the western Indian Ocean; the remaining buoys explored the northern and southern parts of the subantarctic zone (SAZ) from the mid–Indian Ocean (73°E) to the eastern Pacific Ocean (112°W). The air–sea CO_2 fluxes along the buoy trajectories are primarily driven by the spatial variability of the fugacity of CO_2 in seawater, fCO_2: in the SAZ, they vary between -1.1 and -4.2 mol m^{-2} yr^{-1}, and the largest sinks occur close to the STF; in the PZ they vary between -1.6 and 0.6 mol m^{-2} yr^{-1}. When spatially extrapolated over each region, the yearly fluxes amount to -0.8 Pg C yr^{-1} in the SAZ and to -0.1 Pg C yr^{-1} in the PZ, with very small seasonal variation. In winter–spring, the sea-surface salinity and sea-surface temperature indicate mixing with deep water close to the subantarctic front and an episodic signature of north Atlantic deep water close to the polar front (PF). These events are associated with fCO_2 close to equilibrium. On a small scale (of a few km), close to the STF, fCO_2 variations of 1–2 Pa (10–20 μatm) are associated with the presence of compensated mixed layers.

The Southern Ocean, defined as the ocean south of the subtropical front, no doubt plays a significant role in the absorption of atmospheric CO_2, since it is characterized by surface waters which are mostly undersaturated in CO_2 with respect to the atmosphere (Metzl et al. 1999, 2006) and by very strong winds generating the strongest annual air–sea surface CO_2 exchange coefficients over the global ocean (Boutin and Etcheto 1997), and because it covers a very wide oceanic area. In addition, this is an area where climate change might affect ocean absorption of CO_2 (LeQuéré et al. 2007).

However, estimates of the magnitude of this sink vary significantly depending on the methods used to determine it; for instance, Gloor et al. (2003) found a discrepancy of a factor of $\sim$2 between air–sea CO_2 fluxes derived from oceanic inverse models, atmospheric inversions, and estimates from oceanic CO_2 partial pressure, pCO_2, between 58°S and 36°S. In particular, the atmospheric inversions estimates remain inaccurate: for instance, Patra et al. (2005) found the largest uncertainty (1.21 Pg C yr^{-1}) on their flux estimate between 45°S and 60°S, and Baker et al. (2006) report along-term mean flux estimate south of 45°S ranging between -0.28 and -0.55 Pg C yr^{-1} for 1992–1996, depending on the author of the research. On the other hand, pCO_2 oceanic measurements are sparse,

[1] Corresponding author (jb@locean-ipsl.upmc.fr).

Acknowledgments

We thank J. Etcheto for initiating the project of CARbon Interface OCean Atmosphere (CARIOCA) drifter deployments in the Southern Ocean and for constructive comments on data interpretation. We are grateful to L. Beaumont, T. Danguy, and V. Dutreuil from the technical division of the Institut National des Sciences de l'Univers, who supervised the CARIOCA preparations. We also thank K. Currie and N. Metzl for providing reference measurements shortly after the buoy deployment, allowing the verification of buoy calibration during the SOLAS Air–Sea Gas Exchange (SAGE) and Océan Indien Service d'Observation (OISO) experiments. We thank G. Reverdin, F. d'Ovidio and L. Barbero for helpful comments and discussions. We thank A. Lamalle, M. Mallet, O. Klatt, K. Currie and the Sage team, and the *Tangaroa*, *Marion Dufresne,* and *Polarstern* crews for buoy deployments. Microwave Optimal Interpolated sea-surface temperature data were produced by Remote Sensing Systems and sponsored by the National Oceanographic Partnership Program (NOPP), the National Aeronautics and Space Administration (NASA) Earth Science Physical Oceanography Program, and the NASA Reason Discover Project. Data are available at www.remss.com. The altimeter sea surface height maps (available at http://www-aviso.cnes.fr) were produced by the Segment Sol multimissions d'ALTimétrie, d'Orbitographie et de localisation précise/Data Unification and Altimeter Combination System (SSALTO/DUACS) and distributed by the Archiving, Validation and Interpretation of Satellite Oceanographic Data (AVISO) with support from the Centre National d'Etudes Spatiales (CNES). This work was supported by the French programs PROcessus biogéochimiques dans l'Océan et Flux/Flux Air–Mer en CO_2 (PROOF/FLAMENCO) and Les enveloppes fluides et l'environnement / CYcles Biogéochimiques Environnement et Ressources (LEFE/CYBER) contracts, by the Institut Polaire Paul-Emile Victor (IPEV), and by the European Union Integrated project CARBOOCEAN.

although they have greatly improved in recent years, and are biased towards the summer season (Metzl et al. 2006).

The ocean circulation in the Southern Ocean and associated biogeochemical distributions are mainly influenced by the zonal structure of the Antarctic Circumpolar Current (ACC). This eastward circulation is strongly forced by wind (Hughes et al. 1999; Gille et al. 2001; Dong et al. 2006) and the ACC pathway is steered by the bathymetry (Moore et al. 1999; Dong et al. 2006; Sallée et al. 2008*b*). The Southern Ocean is schematically divided into three zones in which the pattern of flow of the ACC varies: from north to south, the subantarctic zone (SAZ), the polar zone (PZ), and the Antarctic zone. These zones are separated by hydrological fronts characterized by the convergence or divergence of water masses and by strong, narrow jets.

Measurements of pCO_2 indicate that very large undersaturations of CO_2 occur in the SAZ (Metzl et al. 1999). Recent extrapolations based on dissolved inorganic carbon and alkalinity data (McNeil et al. 2007) suggest that this region represents a substantial sink (1.1 Pg C yr^{-1} between 40°S and 50°S), about two-thirds of the estimated sink between 40°S and 70°S, but owing to the difficulty of validating this estimate, one conclusion of the paper is that it will be important in the future to better constrain SAZ CO_2 uptake.

In this paper we present new in situ measurements of ocean surface CO_2 fugacity, fCO_2, recorded by drifting buoys that explore the polar zone and the subantarctic zone of the Southern Ocean. A primary difficulty when working with autonomous surface drifters is how to characterize their location with respect to hydrography. Multiple criteria have been defined to identify hydrological fronts, based either on vertical properties (Orsi et al. 1995; Belkin and Gordon 1996) or on surface properties (Dafner et al. 2003). In this paper, we test several methods for identifying the subantarctic front (SAF) from satellite data based either on sea surface temperature (SST) or on sea-level anomaly gradients. We check the consistency of the data with surface salinity variability, because in most cases this is the only independent parameter available along the drifter trajectories. We then look at the variability of CO_2 parameters relative to the location of the fronts. In addition, on a smaller spatial scale, we highlight the variability of carbon parameters and discuss possible origins of this variability.

The paper is organized as follows: methods, large-scale patterns of measurements, regional measurements highlighting processes at work in the variability of fCO_2 at 2-m depth followed by a discussion.

Methods

CARIOCA measurements

CARbon Interface OCean Atmosphere (CARIOCA) drifters measure hourly, at a depth of 2 m, fCO_2, SST, sea surface salinity (SSS), and fluorescence, and at a height of 2 m, surface wind speed (U), atmospheric pressure (Pair), and air temperature (Tair). All the buoys included in this paper measured optical dye absorbance at three wavelengths, ensuring an internal control of the calibration of the CO_2 sensor (Copin-Montégut et al. 2004).

In the past, comparisons of CARIOCA and shipboard fCO_2 measurements have been performed during several campaigns in the North Atlantic and in the Mediterranean Sea (Bates et al. 2000; Hood and Merlivat 2001; Copin-Montégut et al. 2004). All these studies conclude to an absolute precision of CARIOCA fCO_2 close to 0.3 Pa (1 Pa is equal to 1/0.101325 μatm). In the Southern Ocean laboratory calibration and comparisons of CARIOCA fCO_2 with shipboard measurements are indicated in Web Appendix 1 (www.aslo.org/lo/toc/vol_53/issue_5_part_2/2062a1.pdf). They confirm an absolute precision close to 0.3 Pa. This accuracy is comparable to the overall accuracy of shipboard measurements when uncertainties in temperature corrections and equilibration efficiencies are taken into account (Hood and Merlivat 2001). The relative precision of CARIOCA fCO_2 is estimated to be 0.1 Pa (*see* Web Appendix 1). From Seabird manufacturer information, the absolute precision of CARIOCA SST and SSS after 1 yr of measurement is estimated to be 0.002°C and 0.006 respectively. Comparisons with Array for Real-time Geostrophic Oceanography (ARGO) floats measurements in the vicinity of the CARIOCA buoys (not shown) have confirmed an excellent temporal stability of CARIOCA SSS and SST.

CARIOCA drifters are tethered to holey sock drogues centered at 15-m depth. This is intended to reduce the effect of wind on the surface buoy displacement and to improve the coupling between the buoy and the water in order for the buoy to follow surface currents. Nevertheless, trajectories of surface drifters are called quasi-Lagrangian (Emery and Thomson 1997) because surface drifters do not move on a true density surface as they move on a two-dimensional plane rather than on a three-dimensional density surface and they have a small "slip" of the order of a few cm s^{-1} with respect to the advective flow due to Ekman currents (to the north for westerly winds in the Southern Hemisphere) and to wave-driven Stokes drift. Corrections for these effects have been proposed by various authors in order to deduce geostrophic velocity but this is very challenging in the Antarctic Circumpolar Current because large winds and ocean waves produce slip of drogues or displacements by the Stokes drift that are very difficult to estimate (Niiler et al. 2003). Moreover, in case of CARIOCA, we have no control on the presence or not of the drogue and we cannot exclude that, after some time, the buoy loses it. For all these reasons, CARIOCA drifters may cross hydrological fronts and it is necessary to add external information in order to locate CARIOCA trajectories with respect to hydrological structures.

Data are transmitted in real time via Advanced Research and Global Observation Satellite (ARGOS). Eight buoys deployed in the Southern Ocean explored the northern and southern parts of the SAZ over a wide range of longitudes from the mid–Indian Ocean (73°E) to the eastern Pacific Ocean (112°W); one buoy explored the PZ over all the longitudes of the Atlantic Ocean and over the western Indian Ocean (Fig. 1). They measured fCO_2 over 65 months, during all seasons (Fig. 1b). The characteristics

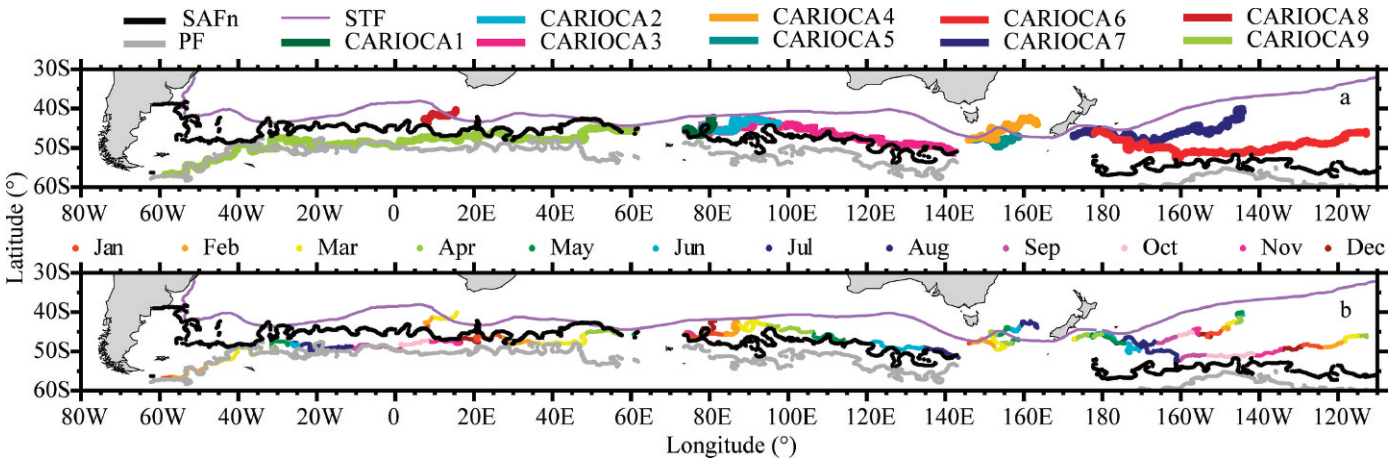

Fig. 1. CARIOCA trajectories in Southern Ocean since 2001 (drifting from west to east) and hydrological fronts: PF, SAFn, and STF; PF and SAFn are detected from altimetry and colocated in time with CARIOCA No. 3, No. 6, and No. 9; STF is a climatological front from Orsi et al. (1995). (a) CARIOCA ID and (b) month sampled by the buoys. CARIOCA drifters No. 1 to No. 8 explore the SAZ, CARIOCA drifter No. 9 explores the PZ.

of each buoy are summarized in Table 1; of the nine buoys, seven buoys measured SSS.

Derived carbon parameters

Dissolved inorganic carbon—In order to get a parameter of the carbon system independent of SST variations, and in order to get quantitative information about carbon compound variability, we derive dissolved inorganic carbon (DIC) from fCO_2, SST, and SSS. We use carbonic acid dissociation constants reformulated by Lueker et al. (2000) and the alkalinity–salinity–temperature relationship established by Lee et al. (2006). The uncertainty with respect to derived DIC is linked to (1) uncertainties with respect to the dissociation constants, which lead to an uncertainty of 4.7 μmol kg^{-1} with respect to DIC (Millero et al. 2006), (2) the accuracy of CARIOCA fCO_2 (0.3 Pa), which produces an accuracy of about 1.5 μmol kg^{-1} on DIC, and (3) the precision of the alkalinity derived from the relationship established by Lee et al. (2006; 8.4 μmol kg^{-1}), which produces a DIC precision of 9.3 μmol kg^{-1}. Taking the square root of the sum of these individual errors, we find an uncertainty with respect to DIC of 10.5 μmol kg^{-1}. This number primarily represents regional biases typically on a scale of 1000 km, because differences between calculated and measured alkalinity vary by region (*see* fig. 2 of Lee et al. 2006); on a kilometric scale, since the relative precision of CARIOCA fCO_2 is 0.1 Pa (*see* Web Appendix 1), relative precision with respect to successive DIC is expected to be 0.5 μmol kg^{-1}.

The air–sea CO_2 fugacity gradient—The air–sea CO_2 fugacity gradient is computed as

$$\Delta fCO_2 = fCO_2 - fCO_2^{atm} \quad (1)$$

where fCO_2^{atm}, the atmospheric CO_2 fugacity, is derived from the atmospheric CO_2 partial pressure, pCO_2^{atm}, Pair, and SST, as detailed, for instance, in (Zeebe and Gladrow 2001):

$$fCO_2^{atm} = pCO_2^{atm} \exp[\mathrm{Pair}(B + 2\delta)/(\mathrm{RSST})] \quad (2)$$

where R is the gas constant, SST is in Kelvin; B and parameter δ are the first virial coefficient for CO_2 and the cross-virial coefficient respectively. B and δ are related to Tair following (Weiss 1974) relationships.

Table 1. Characteristics of CARbon Interface OCean Atmosphere (CARIOCA) drifters in the Southern Ocean. SSS = sea surface salinity; – = SSS data missing; X = SSS data available; OISO = Océan Indien Service d'Observation; SAGE = SOLAS Air–Sea Gas Exchange.

Year	Buoy No.	Ocean sector	Start date of fCO_2 meas.	End date of fCO_2 meas.	Duration (days)	Longitude range	SSS	Ship and pCO_2 campaign for CARIOCA deployment
2001	1	Indian	20 Nov 01	17 Dec 01	27	74°E–81°E	–	Marion Dufresne
2002	2	Indian	13 Jan 02	08 Apr 02	85	74°E–97°E	X	Marion Dufresne and OISO8
2002	3	Indian	13 Jan 02	16 Jul 02	184	74°E–143°E	–	Marion Dufresne and OISO8
2003	4	East Indian	30 Jan 03	01 Sep 03	214	146°E–164°E	X	Marion Dufresne and OISO10
2003	5	East Indian	31 Jan 03	27 May 03	116	146°E–159°E	X	Marion Dufresne and OISO10
2004	6	Pacific	12 Apr 04	20 Apr 05	374	178°E–113°W	X	*Tangaroa* and SAGE
2004	7	Pacific	29 Mar 04	11 Jun 05	440	173°E–144°W	X	*Tangaroa* and SAGE
2005	8	Atlantic	28 Jan 05	31 Mar 05	62	8°E–16°E	X	Polarstern
2006	9	Atlantic	28 Jan 06	08 May 07	466	59°W–61°E	X	Polarstern

pCO_2^{atm} is estimated as

$$pCO_2^{atm} = xCO_2(Pair - Pw) \quad (3)$$

where xCO_2 is the mole fraction of atmospheric CO_2, and Pw is the saturated water pressure derived from CARIOCA SST using the formulation established by Weiss (1974). xCO_2 is derived as

$$xCO_2 = xCO_2(2001) + xCO_2\_trend(year - 2001) + var\_seas(month) \quad (4)$$

where xCO_2 (2001) is taken as equal to the mean annual xCO_2 recorded at Macquarie Island (368.23 μmol mol^{-1}; Steele et al. 2002), xCO_2_trend is taken as equal to the mean annual trend of recent years (1.7 μmol mol^{-1} yr^{-1}), and var_seas (month) is a 10-yr averaged seasonal variation derived from Macquarie Island xCO_2 recorded between 1992 and 2001.

Air–sea CO_2 flux—Flux computed for individual CARIOCA fCO_2 measurement is derived from ΔfCO_2 colocated with weekly $1^\circ \times 1^\circ$ CO_2 exchange coefficients computed from Quick Scatterometer satellite (QSCAT) wind speeds and the short-term k–U relationship established by Wanninkhof (1992), according to the methodology described in (Boutin et al. 2002). We choose to use (Wanninkhof 1992) relationship because it is the most widely used; however, according to new ^{14}C constraints, it is possible that this relationship overestimates K (Naegler et al. 2006; Sweeney et al. 2007), bearing in mind recent measurements made in the Southern Ocean (Ho et al. 2006). Using the k–U relationship established by Ho et al. (2006) would reduce the flux by 22%. For each buoy, fluxes per unit area are averaged seasonally.

Estimates of the seasonal fluxes integrated in the PZ and in the SAZ are derived following two methods. In method 1, the averages of seasonal fluxes per unit area are derived for each buoy in the SAZ and in the PZ respectively. They are multiplied by SAZ and PZ areas which are estimated from the area between the subtropical front (STF) and the northern subantarctic front and between PF and SAFn, respectively, and are seasonally averaged. In method 2, the average of spatially integrated fluxes is derived from monthly fCO_2 values extrapolated over a $1^\circ \times 1^\circ$ grid: in the SAZ, we use fits between fCO_2 and distance to SAF in the SAZ (*see* Results section); in the PZ, we only consider monthly mean fCO_2. ΔfCO_2 is derived using the monthly average of fCO_2^{atm} derived for buoy measurements, making the implicit assumption that fCO_2 in the surface ocean and in the atmosphere increase at the same rate. In the SAZ, monthly K values at $1^\circ \times 1^\circ$ resolution are taken as the monthly averages of K grids between 2001 and 2005 (same temporal coverage as the buoy data); in the PZ, 2006 monthly K values are considered.

Differences between fluxes deduced from these two methods are indicative of the influence of K variability (in method 1 only weekly K variability along buoy trajectories is taken into account while in method 2 K variability over the entire zones are taken into account) and of the influence of the distribution of CARIOCA measurements in the SAZ.

Comparison with climatological Δp—Each month, CARIOCA ΔfCO_2 measurements are colocated with the closest grid point of the corresponding month in the CO_2 partial pressure gradient (ΔpCO_2) climatology of Takahashi et al.(2002). All colocated ΔfCO_2 are averaged at the climatological map resolution ($4^\circ \times 5^\circ$); only pixels with >150 CARIOCA measurements are retained. In following this procedure, we ignore the difference between ΔfCO_2 and ΔpCO_2, which is expected to be much <0.1 Pa, and we assume that ΔfCO_2 did not vary between 1995 (the reference year of the climatology) and the years 2001–2007.

Satellite SST and sea-level anomalies

We use the weekly maps of Advanced Microwave Scanning Radiometer-Earth Obser System (AMSRE) SST available at www.ssmi.com. Sea-level anomalies are Segment Sol multimissions d'ALTimétrie, d'Orbitographie et de localisation précise/Data Unification and Altimeter Combination System (SSALTO/DUACS) results distributed by Archivage, Validation et Interprétation des données des Satellites Océanographiques (AVISO) at www.jason.oceanobs.com (delayed time merged product).

ARGO floats

ARGO measurements are taken from the Coriolis Data Assembly Center; only measurements with a good-quality flag (equal to 1) are taken into account. When using ARGO surface measurements to validate front detection, only SSS measurements taken at a depth of <10 m are taken into account. ARGO locations are colocated with the longitude and month of CARIOCA drifter measurements.

Front detection

We try three methods of detecting the SAF. First, we detect the SAF from the maximum SST gradient for SST between 5°C and 9°C from AMSRE SST maps, according to the criteria of Burling (1961) as reused by Moore et al. (1999) and applied recently by Burls and Reason (2006) in the mid-Atlantic. We look at them only from 2004 onwards, because AMSRE data are not available simultaneously with CARIOCA before 2002 and because the 2003 buoys are a long way from the SAF. Second, we detect the SAF using the altimetric sea-surface height (SSH) according to the method described in Sallée et al. (2008*b*). The SSH is the sum of a climatological SSH field referenced to 1500 m and the sea-level anomaly (SLA) from altimetry. The climatological SSH is computed from the combination of ship and ARGO data. Several fronts and jets occur in the vicinity of the SAF; the SAF defined in Sallée et al. (2008*b*) has been validated with respect to subsurface measurements and corresponds to a southern branch of the SAF, close to the climatological front established by Orsi et al. (1995). In this study, we are interested in the northern edge of the SAF zone as well; hence, we also look at a northern section of the SAF, the

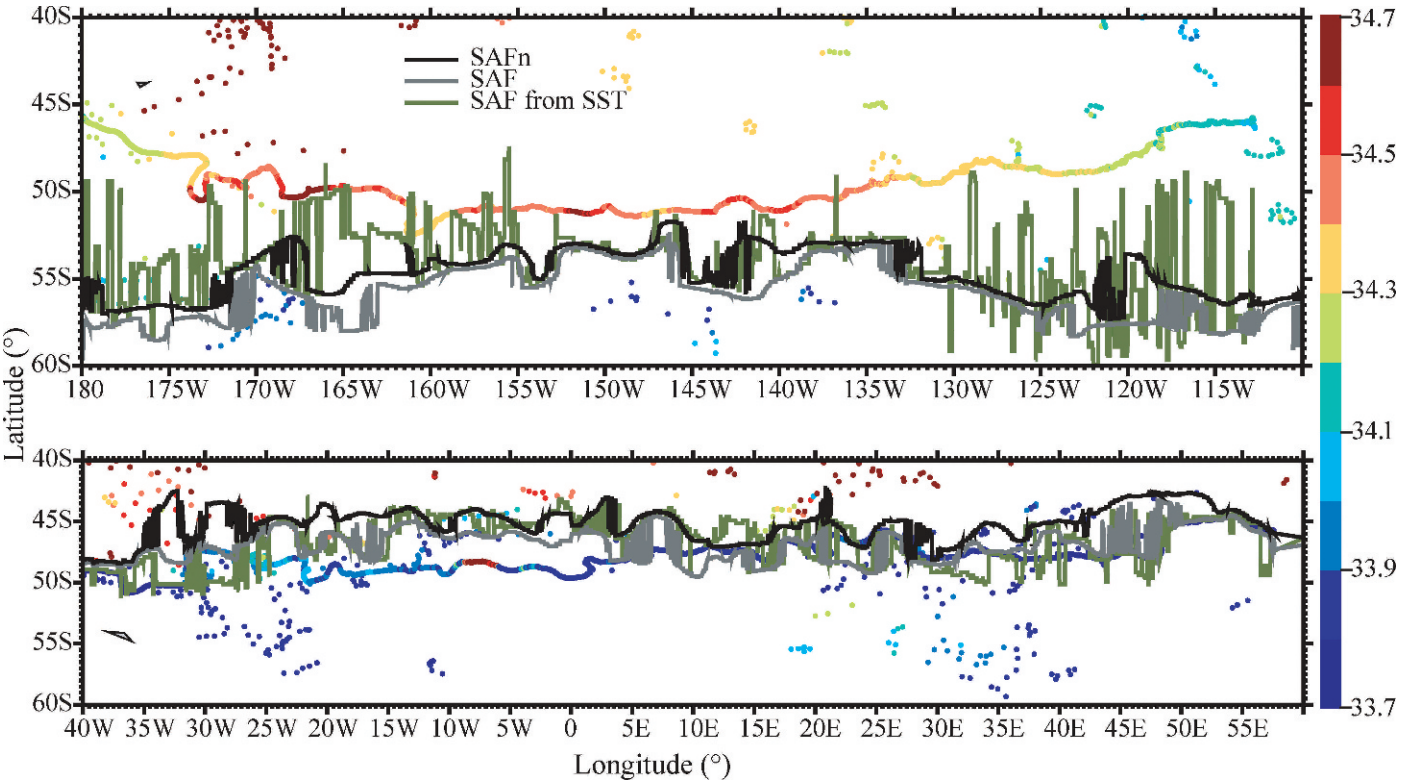

Fig. 2. Subantarctic front detected using three methods: SAFn from altimetry (corresponding to SSH contour of 135 cm); SAF from altimetry (corresponding to SSH contour of 120 cm); maximum SST gradient. These fronts are superimposed on SSS measured by ARGO and CARIOCA. (a) CARIOCA No. 6 in the Pacific Ocean and (b) CARIOCA No. 9 in the Atlantic Ocean. Detection using maximum SST gradient is noisier than detection using SSH contours. SAFn better represents the northern edge of the region with SSS<33.9.

SAFn. Following Sallée et al. (2008*a*) we associated the SAFn to the 135-cm SSH contour (referenced to 1500 m), instead of 120 cm for the SAF.

The three SAF fronts (the SAF from the SST gradient, the SAF and SAFn from altimetry) are colocated in longitude and time (at ±1.5 d for the altimetric SAF and ±3.5 d for the SST gradient SAF) with the trajectory of the buoys.

We analyze the relevance of the fronts detected by these three methods by looking at the longitudinal variability of the SSS as measured by CARIOCA and ARGO floats colocated in longitude and time with CARIOCA buoys (Fig. 2) and SST gradients (Fig. 3). SAF is usually detected from subsurface salinity; however, no salinity profiles are available along CARIOCA trajectories, whereas we observe that the SSS exhibits latitudinal variability in the vicinity of the SAF (as we will show later). In the Pacific, detection of the maximum SST gradient is much noisier than the detection of altimetric fronts in the east and west. In the east, between 130°W and 110°W, very low SST gradients (Fig. 3b) as well as low sea-level anomalies (Sallée et al. 2008*b*) indicate that the SAF is weak. In the west, between 180°W and 160°W, detection of the SST gradient oscillates between SSS equal to 33.9 and to 34.1 (Fig. 2a), because two SST gradients are present in this area (Fig. 3c,d), while the altimetric front more clearly distinguishes water with salinity lower and higher than 33.9 between 175°W and 165°W. In the center of the Atlantic basin (Figs. 2b, 3e,f), the maximum SST gradient is close to the SAFn, whereas it is closer to the SAF east of meridian 0, in the complex area of the Aghulas retroflection. However, east of 30°E, the SAF and maximum gradient detection are noisier than the SAFn. They are sometimes south of low SSS values (<33.9, between 30°E and 40°E), whereas SSS values lower than 33.9 are very rarely seen north of the SAFn. Since it is likely that the SST range in which the SAF is located varies seasonally, we attempted to add a seasonal variation to the SST range in which the maximum SST gradient is determined. However, it was not possible to find a single SST range that applies over the entire circumpolar belt, because the SAF in the Pacific Ocean lies further south than in the Atlantic, and therefore corresponds to a colder SST. The altimetric fronts very often correspond to strong SST gradients: in these regions the surface dynamic is closely linked to the vertical dynamic. Nevertheless, there are some places where the front signature is not seen on the SST gradients (e.g., the eastern Pacific [Fig. 3c,d]). In the present analysis of CARIOCA measurements, we choose the SAFn as the front that best represents the large-scale geostrophic dynamics in the vicinity of the drifters.

The polar front is detected from the SSH and is associated with the 0.95 m contour (Sallée et al. 2008*b*).

Criteria for detecting the subtropical front vary from one author to another; they depend on the region and often

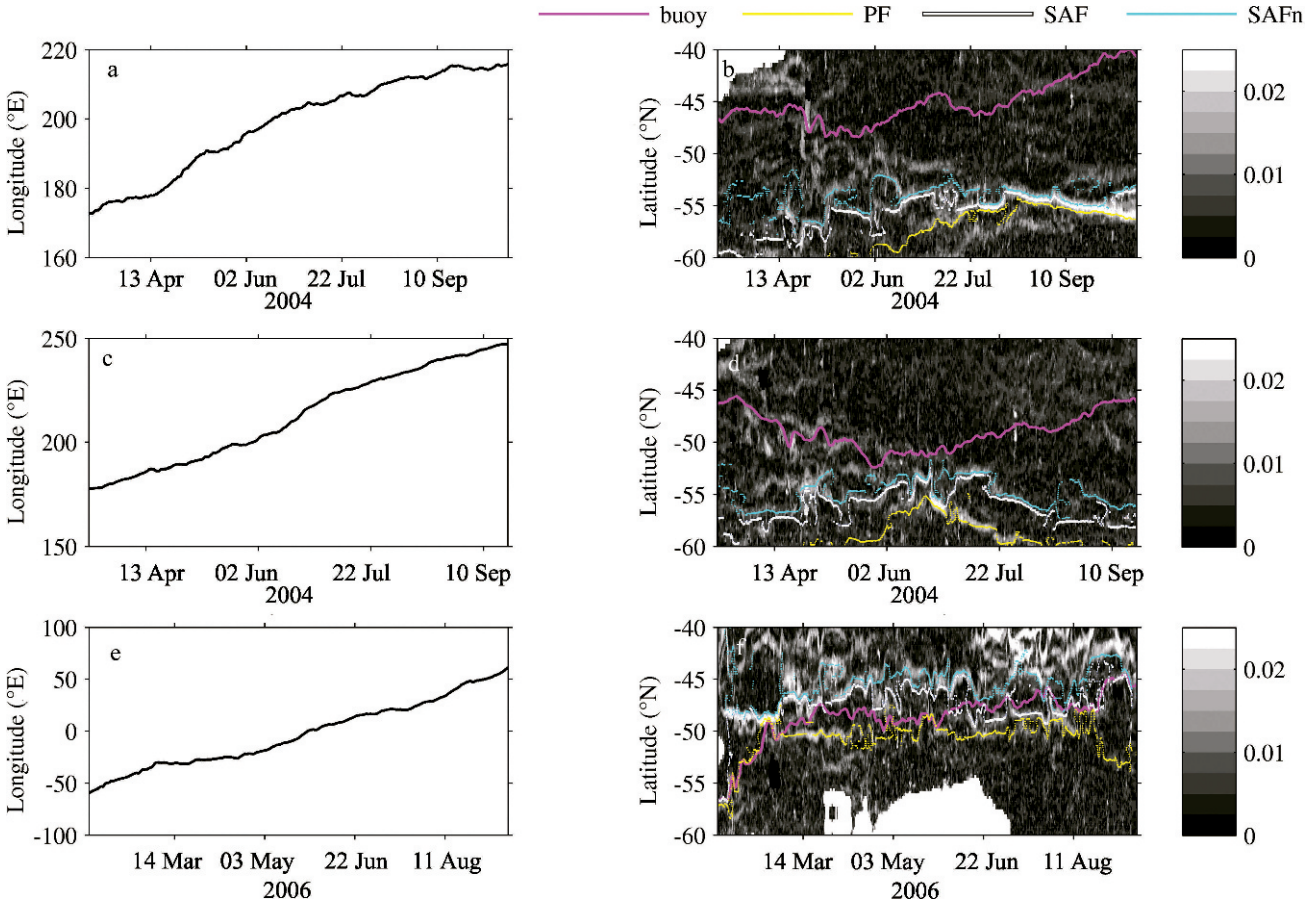

Fig. 3. (a,b) Buoy No. 7; (c,d) Buoy No. 6 and (e,f) Buoy No. 9. (Panels a,c,e) Longitude of the buoy vs. time, and (panels b,d,f) latitude vs. time of the buoy, of the fronts detected from altimetry and colocated in longitude and in time with the buoy. They are superimposed on the SST gradient (black and white scale [units: °C km^{-1}]) colocated with longitude and time of the buoy, between 60°S and 40°S. The altimetric fronts very often correspond to SST gradients but this is not systematic. Buoys trajectories do not systematically follow fronts signature but instead they explore wide areas between fronts.

involve knowing temperature and salinity gradients (Belkin and Gordon 1996). Consequently only the climatological STF front from Orsi et al. (1995) is shown in the figures. The STF front can be identified on the CARIOCA measurements as a SSS front close to 34.9, between 34.6 and 35.1 (Deacon 1982).

Results

Large-scale results

CARIOCA measurements—The buoy locations with respect to the colocated fronts detected from altimetry and from the SST gradients indicate that the buoys follow fronts on some parts of their trajectories, but not at all systematically. In particular, Fig. 3 indicates that buoy No. 9 crosses the PZ and that both buoys No. 7 and No. 6 cross parts of the SAZ of the Pacific Ocean, so that they can be considered to give a synoptic view of the frontal areas.

CARIOCA measurements along the buoy trajectories are presented in Fig. 4. The lowest fCO_2 values, <33.4 Pa, are observed in the SAZ, mostly close to the STF. The highest fCO_2 values, >36.5 Pa, are observed in the PZ in the western South Atlantic in Jan–Feb, in the PZ of the eastern Atlantic and western Indian Ocean from Sep to May, south of the SAZ in the Pacific Ocean in Oct, in the middle of the SAZ east of 120°W in the Pacific Ocean in Mar–Apr, and more occasionally close to the subtropical front in the Atlantic and Indian Oceans. Because of compensation between fCO_2 and the effects of SST on the DIC, DIC variability differs from fCO_2 variability: the highest DIC values are located in the PZ of the central Atlantic Ocean in winter and spring. The maximum DIC stays south of the SAZ in the Pacific in Oct, but local maxima do not appear close to the STF. The lowest DIC values (~2020 μmol kg^{-1}) are located in the SAZ, most commonly in the northern part of the SAZ, close to the STF. From Jul to Dec in the Pacific, fCO_2 and the DIC measured in the southern part of the SAZ are higher than those measured in the northern part.

Given the variability described above, we look at the DIC and fCO_2 as a function of the distance to the SAFn (Fig. 5). In order not to include high fCO_2 values possibly linked to local phenomena occurring close to New Zealand, for this analysis we do not take into account the No. 6

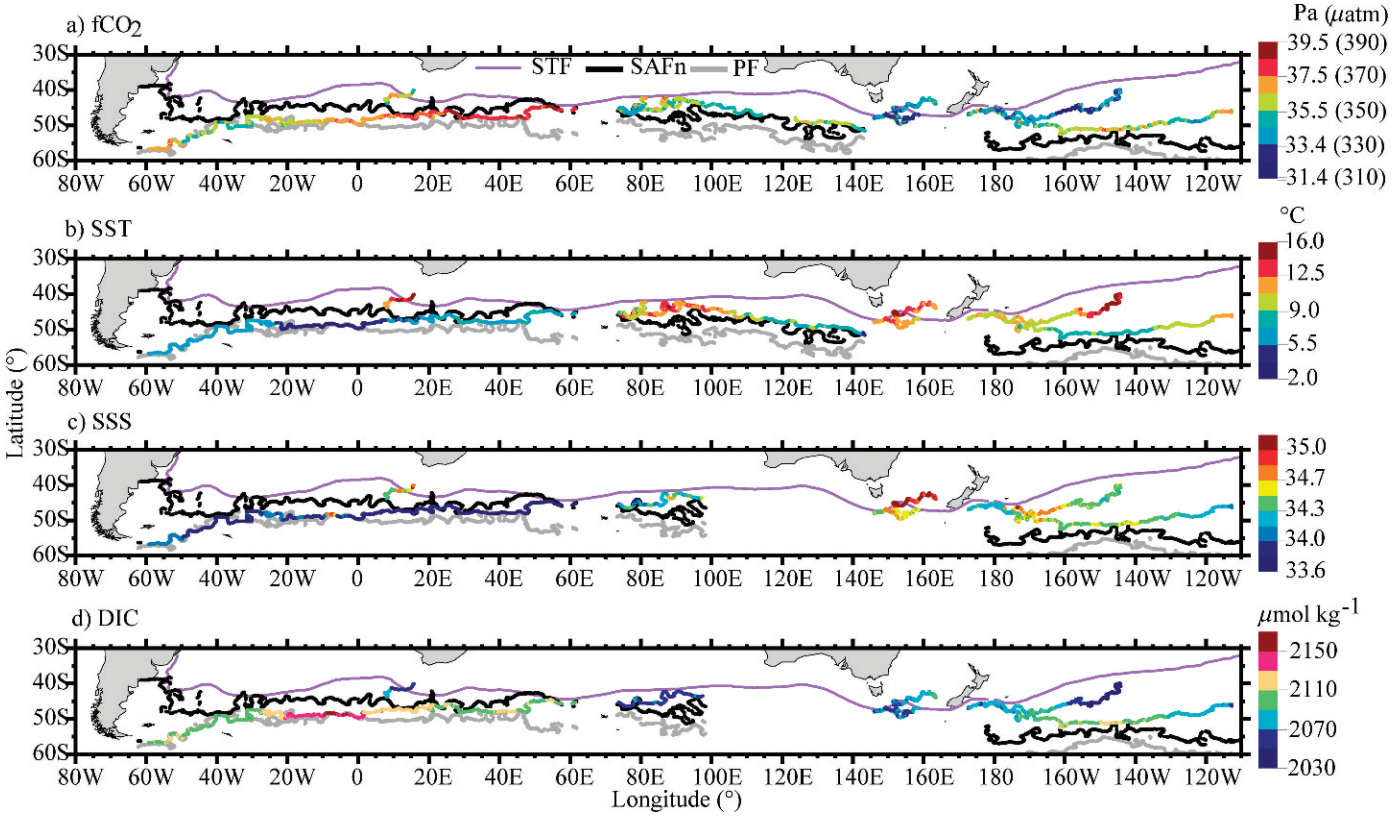

Fig. 4. (a) f CO_2, (b)SST, (c) SSS measurements along CARIOCA trajectories, and (d) DIC derived from above measurements. STF is from Orsi et al. (1995), while SAFn and PF are determined from altimetry and colocated in longitude and time with the southernmost buoys.

buoy data east of 176.8°W or the No. 7 buoy data east of 176.2°E. Close to New Zealand high peaks of fCO_2 values are recorded: four peaks lasting 2–3 d with fCO_2 up to 39.5–42.5 Pa are recorded by buoy No. 6 east of 176.6°W, and one period lasting 2 d is recorded by buoy No. 7 with fCO_2 up to 42.5 Pa east of 176.2°E. The origin of these high peaks is unknown. On the one hand, during these periods all buoy control parameters are correct, so we can trust the spectrophotometer measurements. On the other hand, no unusual indicator is recorded for the SSS, SST, wind speed, and fluorescence parameters. Thus it was not possible to determine whether these high values came from oceanographic phenomena linked to complex bathymetry around New Zealand or from the presence of calcifying organisms in the water surrounding the buoys (we could not identify the presence of coccoliths on Seawifs–Modis satellite images).

In the PZ, the DIC varied by up to 2200 μmol kg^{-1} during one event in Sep between 9°W and 5°W (Fig. 5a–c). This particular event will be discussed later in the regional studies section. Over the rest of the measurements in the PZ, the DIC varies between about 2090 and 2120 μmol kg^{-1}, with minimum values in Mar–Apr and maxima in winter (Jul–Sep). North of the SAF, there is a general decrease in DIC when going from the SAF to the STF. For a given distance to the SAFn, we observe a seasonal variability in the DIC, with DIC maxima between Jul and Oct and minima between Dec and Jun, and greater variability in summer–autumn than in winter. In order to quantify these variations, we compute monthly regression lines between the DIC measured in the SAZ (located north of the SAFn and associated with SSS <34.9) and distance to the SAFn (Fig. 5a–c). The scatter around the regression lines, σ_{DIC}, is minimum in winter (<5 μmol kg^{-1}) and maximum in summer (up to 19.8 μmol kg^{-1}; Table 2). On a yearly average the north–south DIC decrease is −4.9 μmol kg^{-1} °lat^{-1}, with a larger decrease in spring. Between Feb–Mar and Aug, fits are shifted by 29 μmol kg^{-1}.

Concerning fCO_2 (Fig. 5c,e), in PZ, no clear seasonal cycle is observed, nor north–south variability: for the period Mar to Apr, fCO_2 varies between about 35.0 Pa in the western Atlantic to >37.5 Pa in the western Indian Ocean; this variability is probably the result of longitudinal variability. When looking at integrated fluxes in the PZ, we will consider mean monthly fCO_2 representative of the whole PZ.

In the SAZ, for some periods, we observe a decrease of fCO_2 from the SAFn to the STF. We compute monthly regression lines between the fCO_2 (located north of the SAFn and associated with SSS<34.9) and distance to the SAFn (Fig. 5e). As for DIC, we report in Table 2, the scatter around the regression lines, σ_{fCO2}. A seasonal trend is observed in the fCO_2 decrease from the SAFn to the STF, but on fCO_2 averaged over the whole of the SAZ there is no evidence of seasonal variation. From Sep to Jan, fCO_2 significantly decreases from the SAFn to the STF by 0.64 Pa °lat^{-1} while the north–south trend during other

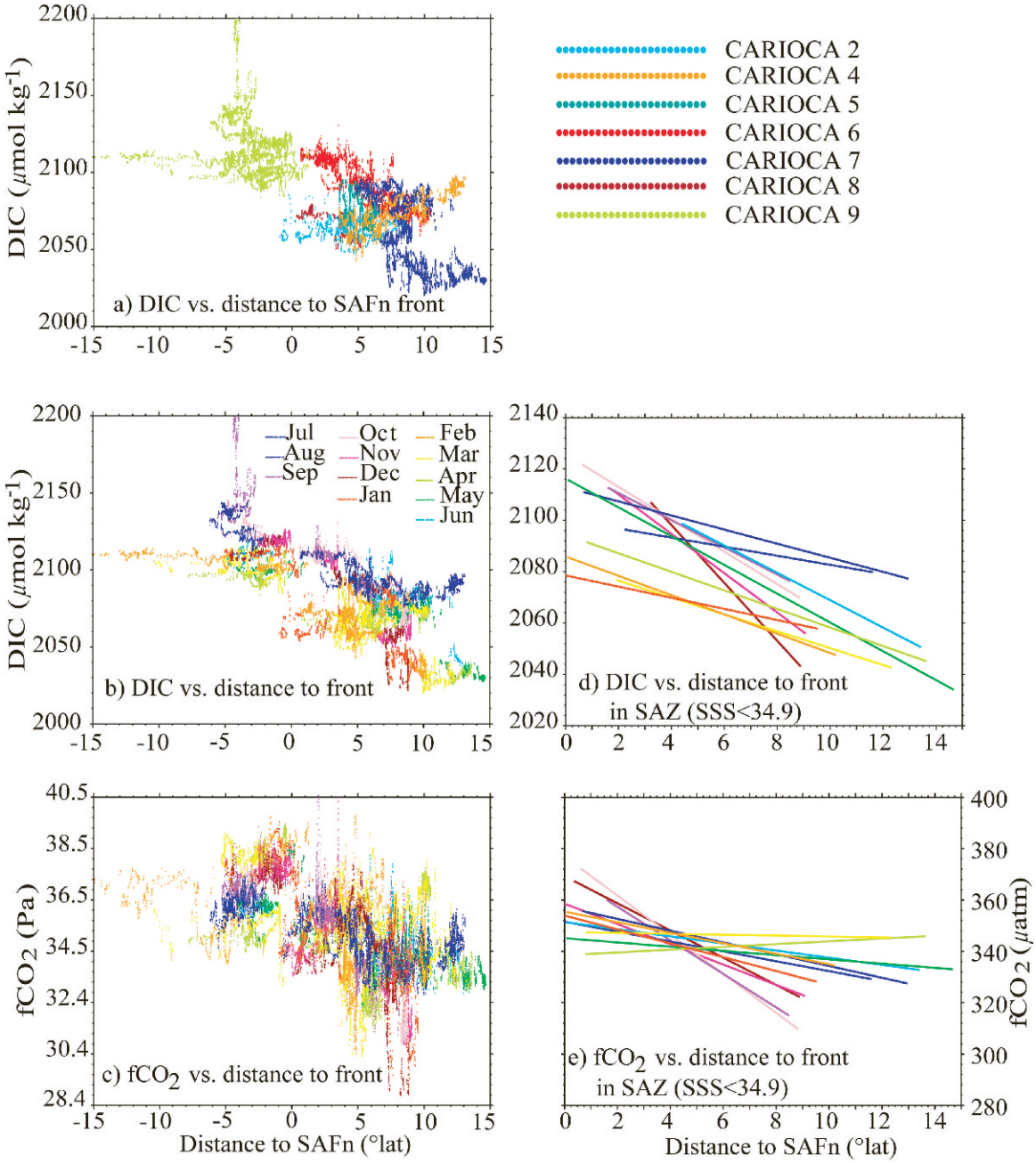

Fig. 5. (a) DIC vs. distance to SAFn color-coded by buoy number (same color code as Fig. 1); (b) DIC vs. distance to SAFn color-coded in months; (c) CARIOCA fCO_2 vs. distance to SAFn color-coded in months. Regression lines computed from data in the SAZ (north of SAFn and SSS<34.9) for (d) DIC, and (e) fCO_2. In the PZ (distances <0), DIC is quite stable except during one event in Sep 2006 (*see* text); no seasonal cycle on fCO_2 nor on DIC can be detected. In the SAZ (distances >0), DIC vary seasonally and decreases from south to north; on fCO_2, the south–north decrease is predominant during winter–spring months.

periods is very small (always <0.2 Pa °lat^{-1}) and is not significant given data scatter around the fits (Table 2). The number of 1° × 1° rasters visited each month by the buoys varies between 20 in Sep and 56 in Mar (Table 2). This is much less than the number of 1° × 1° rasters contained in the SAZ (3600). Nevertheless, these fits are likely to be representative of a much wider area of the SAZ for three reasons: (1) over one month, the CARIOCA measurements are spread in the SAZ over a latitudinal range between 6.5° (in Apr) and 14.5° (in May; Fig. 5c) while the mean latitudinal width of the SAZ is 10°; (2) from one month to another, we observe a continuity in the fits slopes and abscissas while from one month to another the buoys explore different longitudinal regions; and (3) fCO_2 fits were determined from measurements of CARIOCA No. 1 to No. 8 contrary to DIC fits because DIC for CARIOCA No. 1 and No. 3 is not available. fCO_2 fits determined without CARIOCA No. 1 and No. 3 measurements (not shown) are very similar to fCO_2 fits determined with all buoys in the SAZ.

Table 2. Standard deviation of dissolved inorganic carbon (DIC) and fCO_2 with respect to fits shown on Fig. 5.

Month	No. of measurements (DIC)*	No. of buoys (DIC)*	σ_{DIC} (μmol kg^{-1})	No. of measurements (fCO_2)*	No. of buoys (fCO_2)*	No. of rasters (fCO_2)†	σ_{fCO2} (Pa)
Jan	2047	3	19.8	2445	4	33	1.33
Feb	3945	6	12.7	4615	7	40	1.31
Mar	4140	6	14.2	4830	7	56	1.41
Apr	3438	5	15.3	4135	6	41	1.83
May	2695	4	10.2	2925	5	49	1.09
Jun	1917	3	10.9	2000	4	50	0.83
Jul	1481	2	4.9	1712	3	37	0.66
Aug	1544	2	4.7	1544	2	23	0.58
Sep	1434	2	4.5	1434	2	20	0.87
Oct	1488	2	7.0	1488	2	24	0.82
Nov	1441	2	6.9	1665	3	24	1.46
Dec	1489	2	11.6	1887	3	20	1.47

* The number of measurements and the number of buoys used to derive the fits is different for DIC and for fCO_2 because for the two buoys not measuring SSS, DIC was not calculated.
† Number of 1° × 1° rasters visited by CARbon Interface OCean Atmosphere (CARIOCA) drifters.

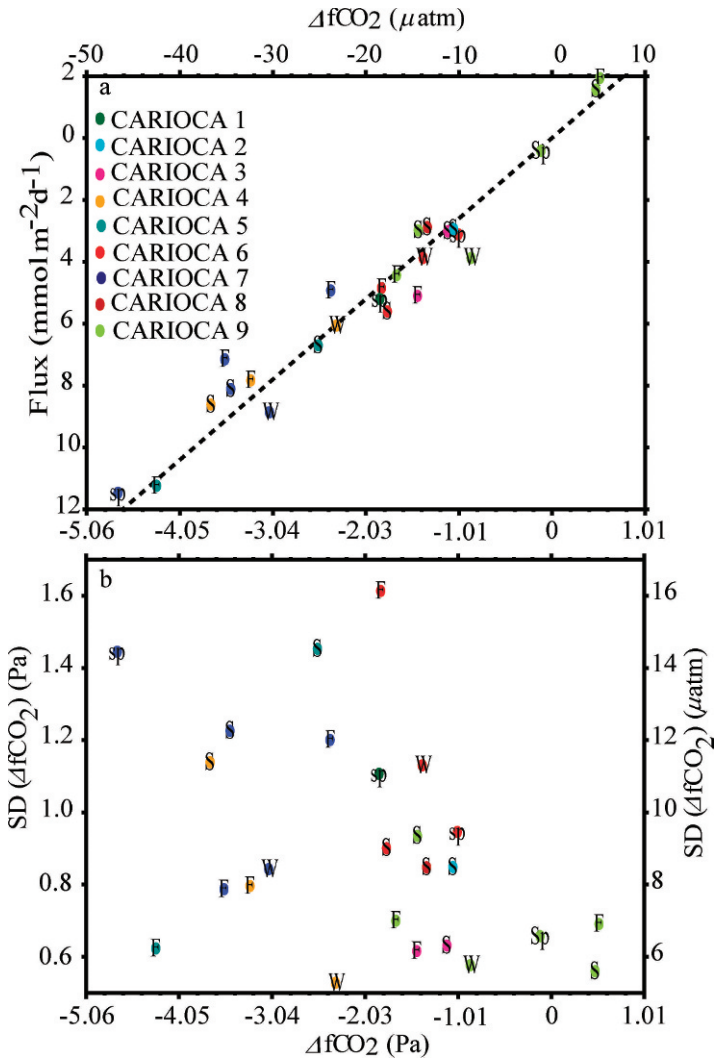

Fig. 6. (a) Flux vs. ΔfCO_2 averaged by season and (b) standard deviation of seasonal Δp; (F: autumn, W: winter, S: summer, Sp: spring); the color code corresponds to the CARIOCA buoy and is the same as Fig. 1. Only periods of >2 months are taken into account, except for buoy No. 1 which lasts for only one month in summer. Seasonal flux is primarily driven by ΔfCO_2.

Table 3. Seasonal air–sea CO_2 flux in the subantarctic zone (SAZ) and polar zone (PZ) averaged by season and by year.

	Jan–Mar	Apr–Jun	Jul–Sep	Oct–Dec	Annual
SAZ					
No. of buoys*	7	8	3	3	8
Longitude extent (°)†	60.7	73.9	41	40.1	148.0
Latitudinal range (°)‡	12.3	14.8	10.5	11.6	14.8
Surface of SAZ (10^6 km^2)	31.3	31.3	30.6	30.7	31.0
Flux in SAZ§ (mmol m^{-2} d^{-1})	−5.4	−5.6	−6.4	−6.6	−6.0
Flux in SAZ§ (Pg C)	−0.18	−0.19	−0.21	−0.22	−0.81
Flux in SAZ‖ (Pg C)	−0.16	−0.22	−0.24	−0.19	−0.81
PZ					
No. of buoys*	2	2	1	1	1
Longitude extent (°)†	49.2	25.3	26.2	20.1	120.8
Latitudinal range (°)¶	5.0	7.4	1.6	2.6	7.4
Surface of PZ (10^6 km^2)	13.7	13.2	13.4	13.6	13.5
Flux in PZ§ (mmol m^{-2} d^{-1})	−0.7	−1.3	−3.9	−0.4	−1.6
Flux in PZ§ (Pg C)	−0.01	−0.02	−0.06	−0.01	−0.09
Flux in PZ‖ (Pg C)	0.01	−0.05	−0.03	−0.02	−0.11

* The same buoy sampling the same season at a 1-yr interval is counted as two buoys in the season.
† Number of longitude degrees visited by the CARbon Interface OCean Atmosphere (CARIOCA) drifters over the period.
‡ Range of distances with respect to the subantarctic front (SAF) visited by CARIOCA drifters over the period.
§ From the average of seasonal fluxes derived from CARIOCA measurements.
‖ From monthly extrapolation of fCO_2 using fits with respect to distance to SAF in SAZ, and from monthly mean fCO_2 in PZ.
¶ Range of distances with respect to the polar front (PF) visited by CARIOCA drifters.

Air–sea CO_2 fluxes—Over the wide area sampled by the buoys, the seasonally averaged variations of the flux (summer: Jan to Mar; autumn: Apr to Jun, winter: Jul to Sep; spring: Oct to Dec) along the buoy trajectories are primarily driven by ΔfCO_2 (Fig. 6): on average there is a factor of 0.026 between ΔfCO_2 (Pa) and flux (mmol m^{-2} d^{-1}), which corresponds (for the k–U relationship established by Wanninkhof [1992]) to a mean wind speed of 10 m s^{-1}. Around this mean line, variation (of up to 2 mmol m^{-2} d^{-1}) of the flux remains, due to variations of K, and there is a tendency for fluxes to fall below the 0.026 line in winter because wind speed increases in winter.

No seasonal cycle of ΔfCO_2 (Fig. 6) can be identified, either in the case of all the buoys, or of only the buoys in the SAZ (all the buoys except buoy No. 9 and No. 4 in autumn and winter), or of the buoy in the PZ (in summer–autumn 2006, the buoy No. 9 sampled the southern Atlantic west of 30°W and ΔfCO_2 was below −1.5 Pa; in summer–autumn 2007, it sampled the Atlantic and Indian Oceans east of 20°E and ΔfCO_2 was around +0.5 Pa). It is in the PZ (buoy No. 9) in the eastern Atlantic and western Indian Oceans that ΔfCO_2 and air–sea CO_2 fluxes are the closest to 0. This is also a region where intra-seasonal variability is relatively small, with standard deviation (SD) of ΔfCO_2 within a season, SD(ΔfCO_2) below 0.7 Pa (Fig. 6b). In the SAZ, SD(ΔfCO_2) always below ΔfCO_2 (Fig. 6b) indicates that the SAZ is mostly a sink over a shorter time scale than a season. It is mostly larger than in the PZ because it varies between 6 and 1.6 Pa; values between 1.2 and 1.6 Pa in autumn and summer correspond to one buoy close to the STF between Tasmania and New Zealand, where satellite chlorophyll images indicate strong and variable biological activity (not shown) and to two buoys east of New Zealand where anomalous peaks of fCO_2 have been observed (*see* previous section).

When buoy seasonal fluxes are averaged together (Table 3, note §), the fluxes per surface area are more absorbent in the SAZ than in the PZ and their ratio is more than a factor 4, except in winter (only one buoy explores the PZ in winter). In the SAZ, the seasonal variation of the fluxes is small, only 20% higher in the winter–spring than in the summer–autumn seasons because of the relatively small K increase in winter; in the PZ larger fluxes in winter are linked both to higher K and to lower ΔfCO_2, but since only one buoy was sampled this season it is difficult to draw a general conclusion. Because the surface of the SAZ is more than twice that of the PZ, when the fluxes are extrapolated over the whole of each region the contrast between the SAZ and PZ is even larger, with fluxes in the SAZ larger by more than a factor of 8 than in the PZ.

In order to look at the influence of the spatio-temporal distribution of the buoys on the seasonal fluxes integrated in the SAZ and in the PZ, we perform a second estimate of the integrated fluxes after having extrapolated fCO_2 in space at $1° \times 1°$ resolution every month. In the SAZ, we apply the fits shown on (Fig. 5e). For distances to the SAFn outside the range covered by the buoys, in order not to exaggerate low fCO_2 values in the northern part of the SAZ, in particular in the eastern Pacific where we do not get data, we use constant fCO_2 values, equal to the closest minimum or maximum fit value. In the PZ, since no tendency with respect to the fronts location was detectable, we only consider the monthly mean fCO_2 from buoy No. 9. On yearly average, fluxes are close to the first estimate (within 0.02 Pg C yr^{-1}); in the SAZ (Table 3, note ‖), the seasonal cycle is slightly higher. The contrast between the fluxes in the PZ, a weak sink, and in the SAZ, a strong sink, remains about the same.

Comparison with climatological ΔpCO_2—ΔpCO_2 and ΔfCO_2 averaged along each buoy trajectory are reported

Table 4. Mean ΔfCO_2 and ΔpCO_2 along CARbon Interface OCean Atmosphere (CARIOCA) trajectories measured by CARIOCA and estimated using the climatology established by Takahashi et al. (2002).

Buoy No.	Mean ΔfCO_2 CARIOCA (Pa)	Climatological ΔpCO_2 (Pa)	CARIOCA ΔfCO_2 − climatology ΔpCO_2 (Pa)	No. of months
1	−1.87	−2.55	0.68	1
2	−1.05	−2.27	1.22	3
3	−1.19	−1.91	0.72	6
4	−3.16	−3.41	0.25	7
5	−3.33	−3.34	0.01	4
6	−1.44	−1.49	0.05	12
7	−3.11	−1.54	−1.58	15
8	−1.38	−2.08	0.70	2
9	−0.60	−2.05	1.45	15
Average*	−18.9	−2.06	0.16	65

* Average is weighted by the number of months of CARIOCA measurements.

in Table 4. Except for buoy No. 7, averaged climatological ΔpCO_2 are smaller than CARIOCA ΔfCO_2.

In the Pacific Ocean, both the climatology and CARIOCA indicate a maximum of ΔpCO_2 close to equilibrium with the atmosphere near 50°S, decreasing in a northerly direction. However, large differences between the No. 7 buoy and climatology occur in the middle of the SAZ (Fig. 7). This discrepancy occurs in a region with a large variability in ΔfCO_2 (Fig. 7c). Between Tasmania and New Zealand, close to the subtropical front, both estimates agree, with a ΔpCO_2 close to −3.5 Pa. In the southern Atlantic both estimates see an east–west gradient, but climatological values are more variable than buoy measurements.

We also report the variability in 4° × 5° pixels of CARIOCA ΔfCO_2 used in these comparisons (Fig. 7c). Large variability occurs south of Tasmania and in the western Pacific; this may be due to complicated hydrography in these areas as well as to the presence of two buoys in the same pixel, performing measurements several hundreds of kilometers apart. West of 176°W, large peaks of fCO_2 (*see* section describing CARIOCA measurements) add to this variability.

Comparison with other studies—Metzl et al. (1999) combined data from 1992 to 1995 from 30°E to 160°E in the SAZ of the Indian Ocean and studied the seasonal cycle of pCO_2; they observe pCO_2 close to equilibrium with the atmosphere in winter and an air–sea disequilibrium close to −70 (in the central Indian Ocean) and to −3.5 Pa (in the eastern Indian Ocean) in summer. Our fCO_2 data, recorded by two drifters in the central Indian Ocean and averaged in summer, indicate a mean disequilibrium of −1.8 and −1.0 Pa ± 0.9 Pa. This apparent discrepancy cannot be explained by problems in the measurements calibration because CARIOCA measurements were in agreement with Océan Indien Service d'Observation (OISO) measurements taken in Jan 2002 at the buoy deployment (*see* Web Appendix 1). On the other hand, SST measured by CARIOCA are often 1–3°C lower than the mean monthly values in 1° × 1° reported by Metzl et al. (1999) in their fig. 5. This may be because CARIOCA drifters sampled a very small latitudinal band close to SAF. Therefore, the smaller disequilibrium (in absolute value) observed by CARIOCA could be because they drifted close to SAF where the mixing of several water masses occurs (as shown in regional studies), whereas the north–south variability in the SAZ has been shown to be large. Further measurements are needed to better understand the reason of this smaller disequilibrium (in absolute value) and before any conclusion about inter-annual variability between 1992–1995 and 2002 can be drawn. On the other hand, measurements taken in the northern part of the SAZ between Tasmania

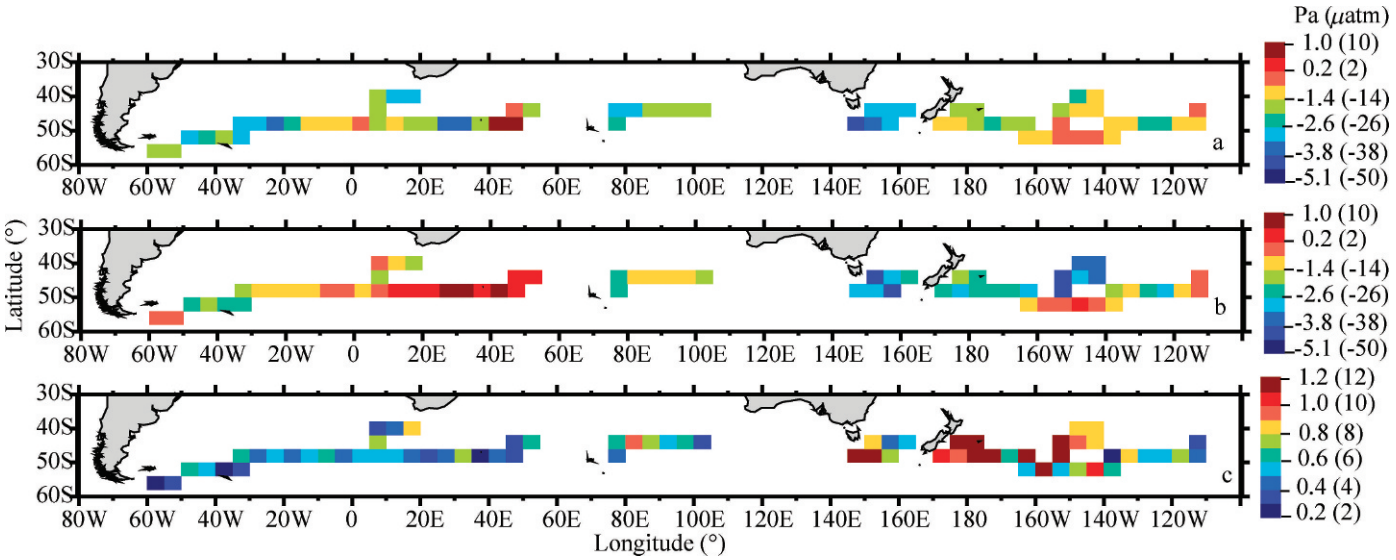

Fig. 7. (a) Climatological ΔpCO_2 colocated with CARIOCA measurements (same months as in Fig. 5); (b) CARIOCA ΔfCO_2 at the same resolution as the Takahashi climatology; (c) standard deviation of CARIOCA ΔfCO_2 in 4° × 5° boxes. Large-scale patterns of CARIOCA ΔfCO_2 are mostly consistent with the climatology given the variability observed in 4° × 5° rasters by CARIOCA drifters.

and New Zealand indicate a mean disequilibrium of -2.5 ± 1.5 and -3.7 ± 1.1 Pa, consistent with the eastern Indian Ocean measurements shown in Metzl et al. (1999) and the 2002 measurements reported by Breviere et al. (2006).

Metzl et al. (1999) observe an anticorrelation between pCO_2 and SST, partly due to a decrease of SST in winter associated with an increase of pCO_2. In our measurements such an anticorrelation is not visible; this may be because in the areas explored by the buoys, SST variations due to spatial variability are of the same order of magnitude as SST variations linked to seasonal variability. CARIOCA data in the SAZ in winter were acquired by two buoys in the Pacific Ocean. The fCO_2 data measured by the southern buoy show an increase of fCO_2 during Aug to Nov when the buoy was the closest to the SAFn. Because of these maximum values, probably associated with the formation of mode water in winter–spring, seasonal mean fCO_2 vary by a factor of 1.5 between summer–autumn and winter–spring. However, the buoy in the northern part of the Pacific SAZ does not exhibit such a decrease in winter, because it is outside the region of mode water formation.

Chierici et al. (2004) reported measurements of fCO_2 from Dec 1997 to Feb 1998 in the Atlantic Ocean between 5°E and 10°E, showing an undersaturation of fCO_2 along the PF of about -2.0 Pa, values close to the equilibrium with the atmosphere close to the SAF and close to the STF, and undersaturation of about -1.0 Pa in the SAZ. In Jan–Feb, between 15°E and 30°E, CARIOCA No. 9 measured fCO_2 close to the equilibrium close to the SAF in the PZ; during the same months, between 8°E and 10°E, CARIOCA No. 8 measured fCO_2 around 35.5 Pa in the SAZ with an increase up to 37.5 Pa, thus close to equilibrium with the atmosphere, when approaching the STF.

Regional studies

Sub-mesoscale variability in the frontal area

Buoy No. 7—In winter 2004, buoy No. 7 was close to the STF in the Pacific Ocean, characterized by a strong SST gradient, as can be seen on AMSRE SST (Fig. 8a), and by a strong sea-level anomaly (Fig. 8b). From 11 Jul to 26 Jul, sharp fCO_2 variations of >1.0 Pa are observed on a kilometric scale with maxima typically extending over 20 km (Fig. 8e). The maximum at 173°W can be explained by the SST anomaly because it is not visible on calculated DIC (Fig. 8f). On the other hand, maxima at 172°W and 169.5°W still correspond to DIC maxima (variations of 8 μmol kg^{-1}). In order to explain these variations, we look at ARGO profiles taken in the region when the buoy was present.

Two ARGO profilers performed measurements at the ocean surface on each side of the CARIOCA trajectory, float A244 in an anticyclonic eddy on 17 Jul and float A444 in a cyclonic eddy on 14 Jul (Fig. 8a,b). On their vertical profiles (Fig. 9), the layer of mixed density is 220 m deep for float 244 and 170 m deep for float 444. However, mixed temperature and salinity layers are much shallower, and a density-compensated layer appears between 170 m and 220 m for A 244 and between 80 m and 170 m for A444.

During that period CARIOCA SSS and SST are aligned onto two isodensities (about 1026.58 and 1026.64 kg m^{-3}). Variations of salinity and temperature observed by the two ARGO floats in the layer of mixed density are aligned along SSS and SST measured by the CARIOCA drifter at a depth of 2 m (Fig. 10b), each Argo float sampling one of these isodensities. CARIOCA DIC maxima are associated with pairs of salinity and temperature observed at the base of the compensated layer by ARGO. This observation suggests a deep origin (in the range of 150–220 m) for the surface DIC maxima observed by CARIOCA. These deep DIC maxima may be due to carbon remineralization in subsurface waters, following strong biological productivity on the surface during summer and autumn.

Buoys No. 2 and No. 3—These two buoys drifted very close to each other for almost three months. They observe strong small-scale variability in fCO_2: when the two buoys were close to the SAFn (Fig. 11a), close to 79°E, a 2.0 Pa difference was observed between the buoys south and north of the front over a distance of ~30 km. However, large variability of fCO_2 also occurs across the SAZ: buoy No. 2 left the SAFn at about 80°E and reached the STF at 87.5°E (SSS >34.5); when crossing the SAZ it recorded fCO_2 varying between 34.5 Pa and 38.0 Pa. Similar variability is observed between the two buoys when at the same longitude.

On the SST–SSS diagram of buoy No. 2 (Fig. 12; buoy No. 3 did not measure SSS), low SSS and SST values in the vicinity of the SAF (close to 79°E) are associated with high DIC (~2085 μmol kg^{-1}), whereas high SSS and SST in the vicinity of the STF (close to 88°E) are associated with low DIC values (~2055 μmol kg^{-1}). Mixing lines appear as expected from water masses mixing in frontal areas. Between SSS = 34.1 and 34.2, corresponding to the buoy between 85°E and 87.5°E, a warming of 2°C occurs, which leads to an increase of fCO_2 of about 3.0 Pa (Fig. 11a), while DIC does not vary, indicating a thermodynamic effect.

DIC in the region of formation of subantarctic mode water (the South Pacific SAZ)

From 10 Sep to 30 Oct 2004, buoy No. 6 was close to the SAFn (Fig. 3c,d), where calculated DIC is higher than over the rest of its trajectory (Fig. 4d). During that period SSS and SST are well-aligned, indicating a mixing of different water masses, and there is a tendency for colder, fresher water to correspond to the highest DIC (Fig. 13). This takes place in a region of formation of subantarctic mode water during winter corresponding to the deepest mixed layer (Aoki et al. 2007).

LCDW signature in the Atlantic Ocean

From 12 Sep to 18 Sep 2006, close to 49°S, 9°W–5°W (i.e., close to the mid-Atlantic ridge and to the polar front), CARIOCA No. 9 recorded very high SSS (between 34.5 and 34.9) and very low SST (between 1.2°C and 2°C; Fig. 14a). During that period, however, no particular signature is

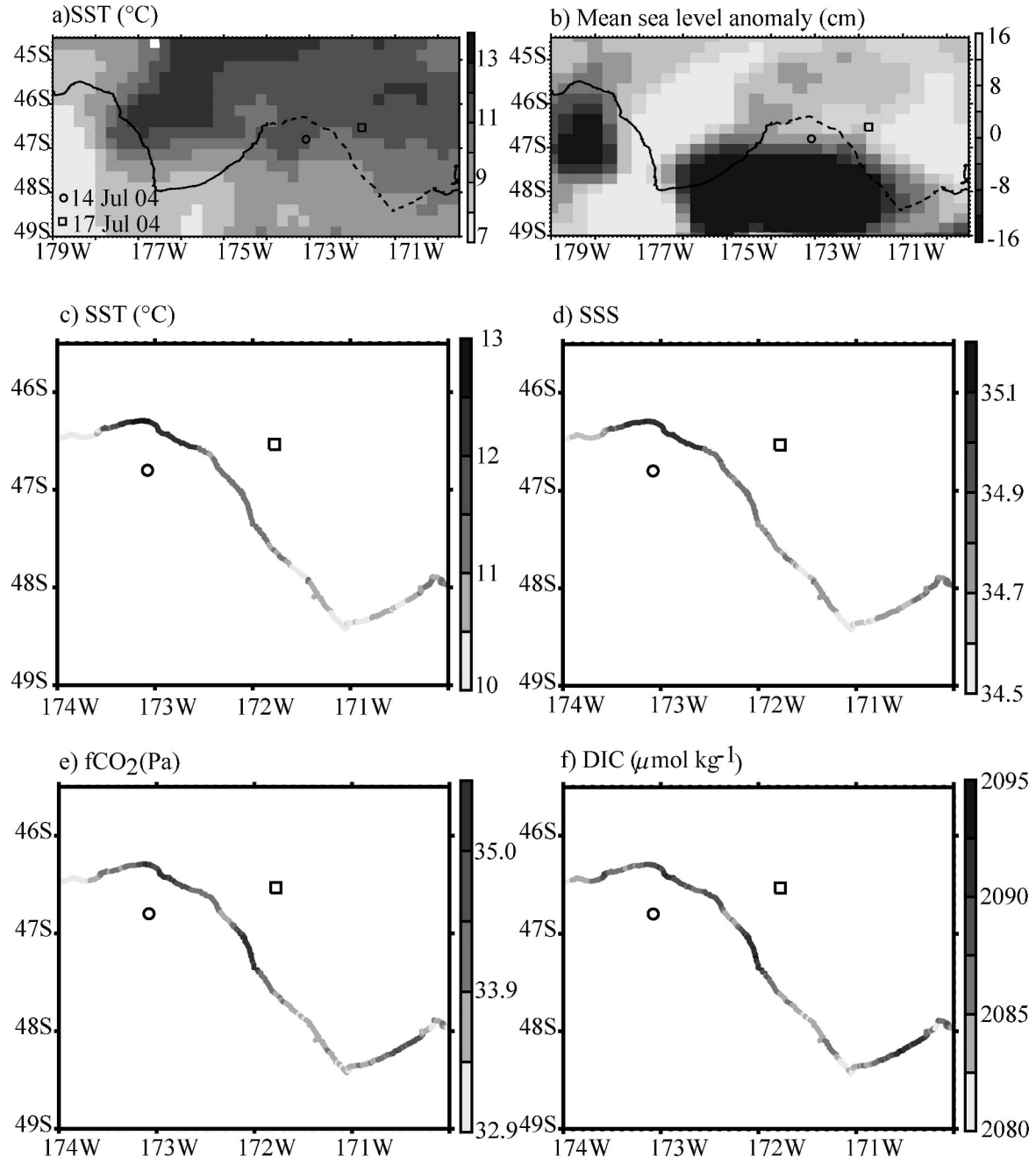

Fig. 8. Sub-mesoscale variability close to subtropical front. (a) AMSRE SST and (b) sea-level anomaly satellite maps on 21 Jul 2004; the CARIOCA trajectory crossing the map is indicated by a solid line; dashed line corresponds to the CARIOCA trajectory between 11–26 Jul. Middle and bottom: CARIOCA No. 7 measurements from 11 Jul to 26 Jul 2004: (c) SST; (d) SSS; (e) fCO_2; (f) DIC; symbols indicate ARGO float SSS measurement from 14 and 17 Jul 2004.

observed for fCO_2 (Fig. 14b); on the contrary, due to the SST and SSS variations, estimated DIC (Fig. 4d) increased by >50 μmol kg^{-1} and ranged between 2180 and 2205 μmol kg^{-1}.

The low SST observation is confirmed on AMSR SST maps from 13 Sep to 22 Sep, the maximum of the anomaly being observed on 15 Sep (Fig. 15). Earlier and later images (not shown) indicate that SST lower than 1°C appears on 13 Sep and that the presence of the cold water at the surface lasts for only 10 d.

The 34.5–34.9 salinity range corresponds to lower circumpolar deep water (LCDW), generally observed between a depth of 1000 m and 3000 m (Olbers et al. 2004). Close to our anomalous surface observations, at 8°W, 50°S, the signature of LCDW (potential temperature of 2°C and salinity of 34.7) was even observed at 800 m (Orsi and Whitworth 2005–2006). Over the A16S line in Jan 2005, salinity of 34.85 was measured at 30°W, 45°S at 2500 m together with a DIC of 2210 μmol kg^{-1} (Wanninkhof et al. 2006). Given the uncertainty of our DIC

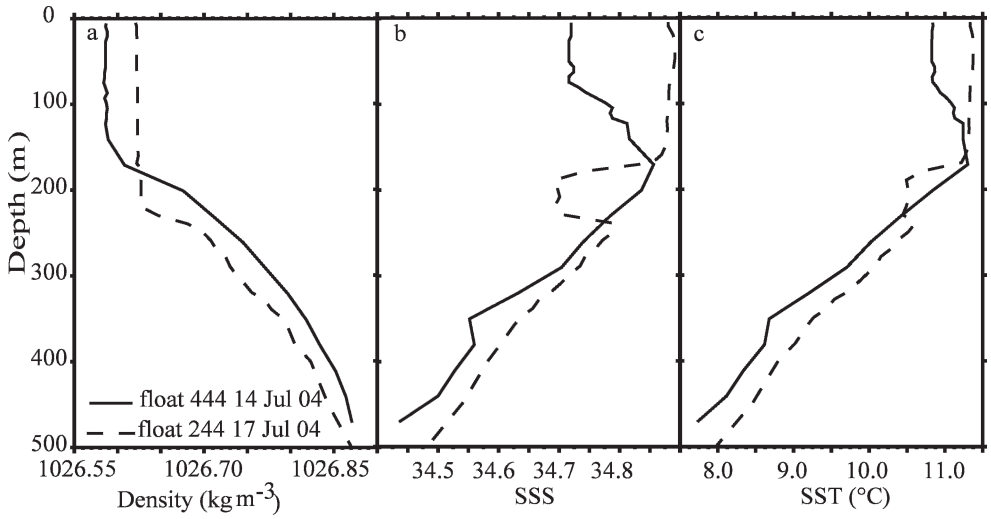

Fig. 9. Vertical profiles of float A444 and of float A244. (a) Density, (b) salinity, and (c) temperature. Density compensated layers are observed between 80 m and 220 m.

calculations (10.3 μmol kg^{-1}), CARIOCA observations support the hypothesis of LCDW outcropping at the ocean surface for 10 d close to 49°S, 9°W–5°W.

Discussion

The measurements of nine CARIOCA buoys widely spread over the SAZ and the PZ of the Southern Ocean allow us to propose new estimates of the yearly air–sea CO_2 flux in these two regions: −6.0 mmol m^{-2} d^{-1} in the SAZ and −1.6 mmol m^{-2} d^{-1} in the PZ. If these numbers are extrapolated over all these regions, the fluxes amount to −0.8 Pg C yr^{-1} in the SAZ and −0.1 Pg C yr^{-1} in the PZ. This confirms the crucial role of the SAZ with respect to the air–sea CO_2 flux in the Southern Ocean. These numbers are calculated using the k–U relationship established by Wanninkhof (1992), in order to remain consistent with other estimates; however, recent studies indicate that this relationship could be too high by 22% (Ho et al. 2006) so that a lower range for the yearly air–sea CO_2 flux extrapolated from CARIOCA measurements is −0.7 Pg C yr^{-1} in the SAZ and −0.1 Pg C yr^{-1} in the PZ.

Another uncertainty arises from the spatial distribution of CARIOCA drifters in the SAZ and in the PZ. In order to estimate the effect of the irregular sampling of the SAZ by CARIOCA drifters, we try two methods to compute extrapolated fluxes and we obtain yearly fluxes in very close agreement (*see* Table 3, flux with notes § and ‖). Nevertheless, both methods only use CARIOCA measurements and we cannot exclude other errors coming from the undersampling of CARIOCA drifters. In the PZ, the buoys perform measurements in all seasons over the Atlantic and eastern Indian Oceans; in the SAZ, during each season, the buoys explore one-ninth to one-sixth of the SAZ longitudes (Table 3, line 2), and cover a range of distances to the SAFn larger than the mean latitudinal width of the SAZ (10°; Table 3, line 3). It will be necessary in future to combine them with ship measurements in order to refine flux estimates and link any uncertainty in the fluxes to

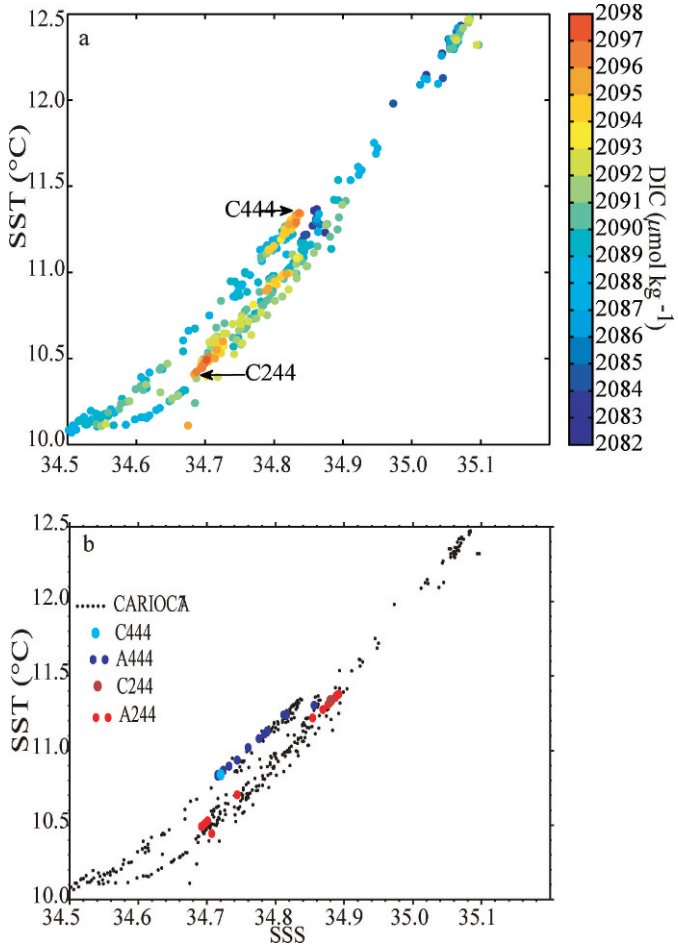

Fig. 10. SST vs. SSS: (a) DIC retrieved from CARIOCA measurements from 11 Jul to 26 Jul, and (b) measurements of CARIOCA from 11 Jul to 26 Jul (black filled circles) and of ARGO floats A444 and A244 in density-mixed layer. Point C444 and point C244 (arrows) indicate SSS and SST measured at the base of the compensated layer by floats 444 and 244 respectively; they correspond to SSS and SST observed by CARIOCA together with DIC maxima.

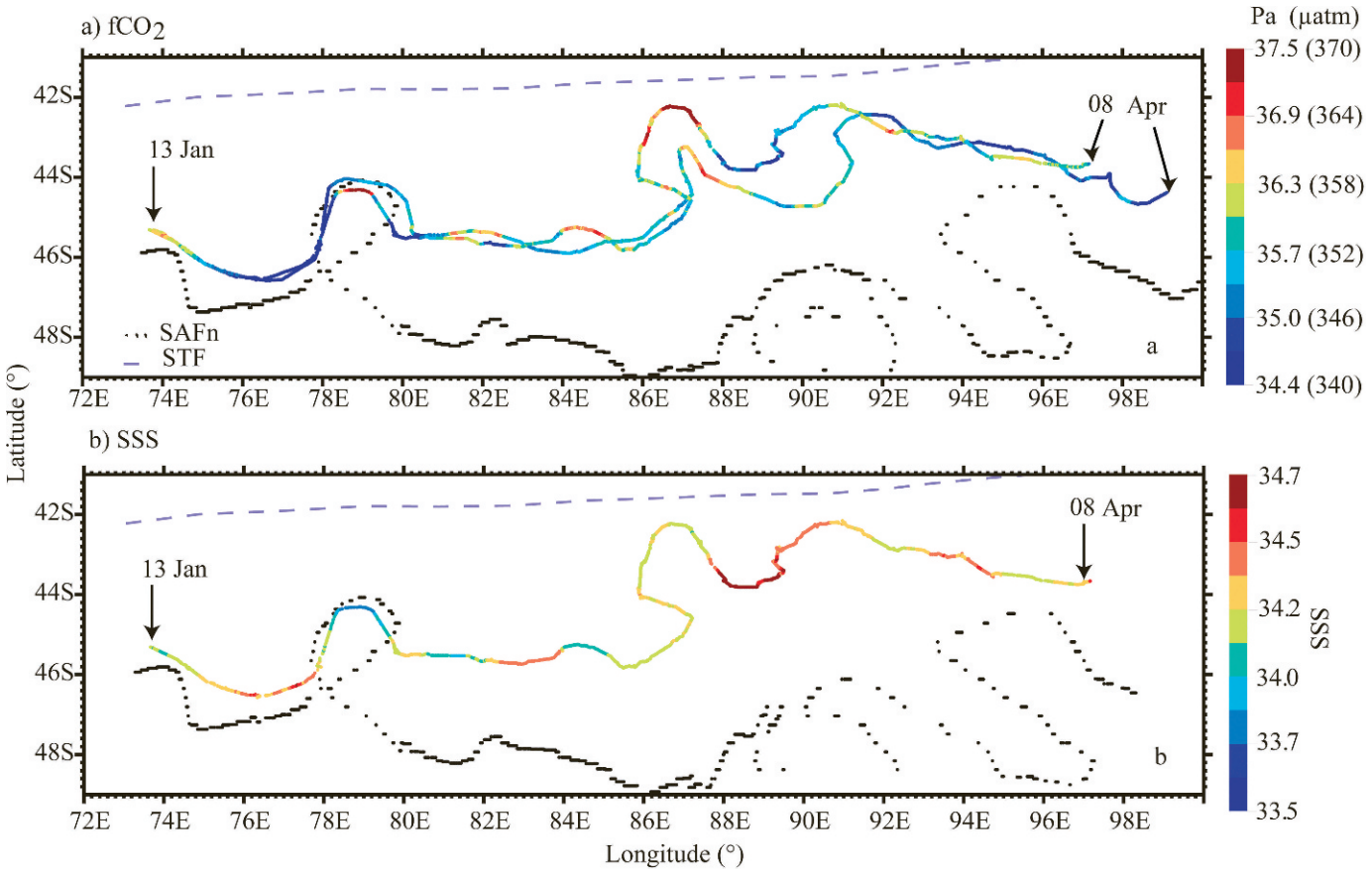

Fig. 11. Small-scale fCO_2 variability observed by two buoys close in space and time. (a) fCO_2 measured by drifters No. 3 and No. 2 from their deployment through 08 Apr 2002, and (b) SSS measured by the drifter No. 2. The Orsi climatological front and the SAFn colocated in time with longitude of CARIOCA drifters are also shown on both panels.

fCO_2 variability. The biggest uncertainty probably arises from undersampling in the Pacific Ocean, because this is the region where the SAZ is the furthest north, where CARIOCA measures a large fCO_2 north–south gradient in winter–spring, and where no measurements were performed by CARIOCA in the eastern sector.

Colocations with ΔpCO_2 climatology (Takahashi et al. 2002) indicate very little bias with respect to CARIOCA ΔfCO_2 on average over all the buoys (0.16 Pa). However, for most buoys, ΔpCO_2 climatology is more negative than CARIOCA ΔfCO_2. These comparisons have to be used with caution, for several reasons: (1) in the Southern Ocean, Takahashi et al. (2002) did not correct pCO_2 data for the atmospheric trend south of 50°S in the Atlantic, Indian, and western Pacific Oceans west of the date line, or south of 60°S in the Pacific Ocean east of the date line, whereas they recently found that data in these regions should have been corrected (T. Takahashi et al. in press). Although CARIOCA data were not collected in these regions except for buoy No. 9 in the Atlantic west of 30°W, we can extrapolate to argue that this correction may affect pCO_2 north of this zone, and that therefore the comparisons presented here have to be used cautiously close to 50°S east of the date line; (2) It is very likely that in the Atlantic and Indian Oceans the proximity of the fronts introduces very great variability in the fCO_2 in 5° × 4° pixels, because several zones can be included in a single pixel; (3) Interannual variability has not been taken into account.

Qualitative comparisons between CARIOCA and ship fCO_2 measurements, located close together and taken in the same season, in the Atlantic and Indian Ocean sectors of the SAZ and PZ, show a fair amount of agreement: fCO_2 is close to equilibrium in the PZ, except in summer close to the PF; fCO_2 is undersaturated with respect to atmospheric value in the SAZ in most periods. Nevertheless, CARIOCA measurements highlight some features not previously evidenced in ship fCO_2 data: in winter–spring, fCO_2 is close to equilibrium near the SAF, probably due in some way to deep-water convection in winter, as already suggested by Metzl et al. (1999), but this observation does not extend over the whole SAZ, in particular in the Pacific Ocean, because areas of formation of subantarctic mode waters in winter do not extend over the whole SAZ (Aoki et al. 2007). On average over the SAZ, no seasonal variation can be identified on fCO_2; CARIOCA fCO_2 data indicate a decrease of fCO_2 from the SAFn to the STF from the end of winter to the beginning of summer (0.63 Pa $°lat^{-1}$), which was not noted in previously published ship data; this may be because few north–south ship transects were taken during these periods and because most north–south transects were performed in areas where the distance between the SAF and the STF is relatively small: we find

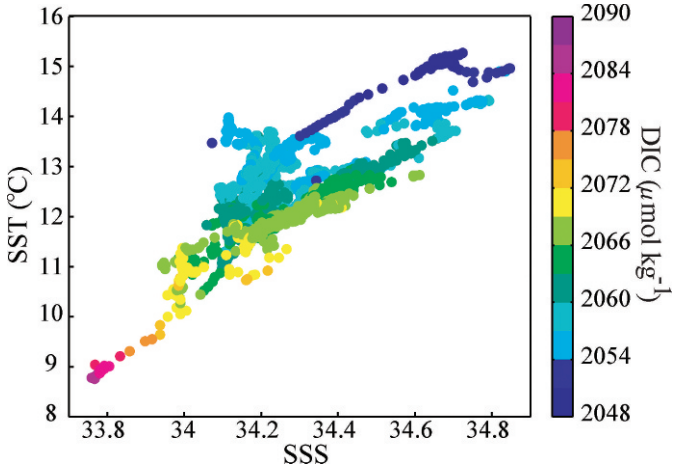

Fig. 12. SST–SSS–DIC diagram of CARIOCA No. 2 when it goes from the vicinity of SAFn to STF (Jan–Apr 2002).

that the standard deviation of fCO_2 with respect to the north–south trend is up to 1.4 Pa in Jan, so that it is very difficult to distinguish between small-scale fCO_2 variability and a north–south trend over distances $<5^\circ$ in latitude. CARIOCA observations also indicate a larger decrease of DIC from the SAFn to the STF in spring, possibly linked to a larger biological uptake during the spring growing season, and a clear seasonal variation of DIC in the SAZ with maxima in winter.

The features drawn from CARIOCA observations are in very close agreement with the conclusions drawn by McNeil et al. (2007). McNeil et al. (2007) studied ship measurements of DIC and Alk since 1986 south of 40°S, and proposed to extrapolate them using standard hydrographic properties. From their extrapolations and using k–U relationship established by Wanninkhof (1992), they estimate a flux of 1.1 ± 0.6 Pg C yr^{-1} within 40°S–50°S, an area geographically close and equivalent in size to the SAZ considered in our paper, and a much weaker sink south of 50°S. They estimate mean annual fCO_2 in the PZ at

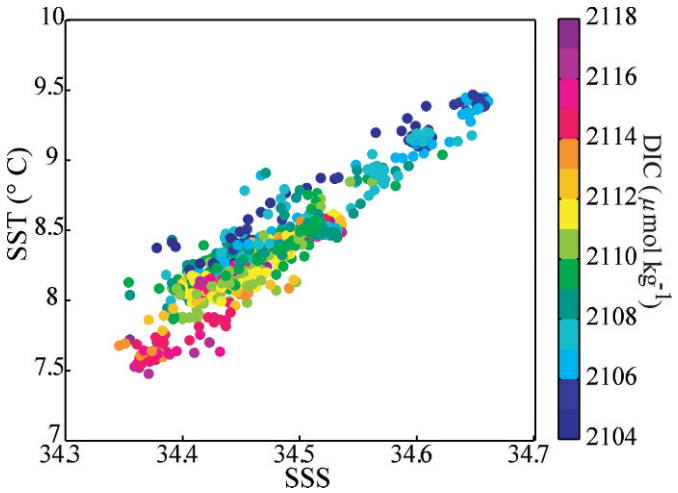

Fig. 13. SST–SSS–DIC diagram of CARIOCA No. 6 when it was close to SAFn (10 Sep–30 Oct 2004).

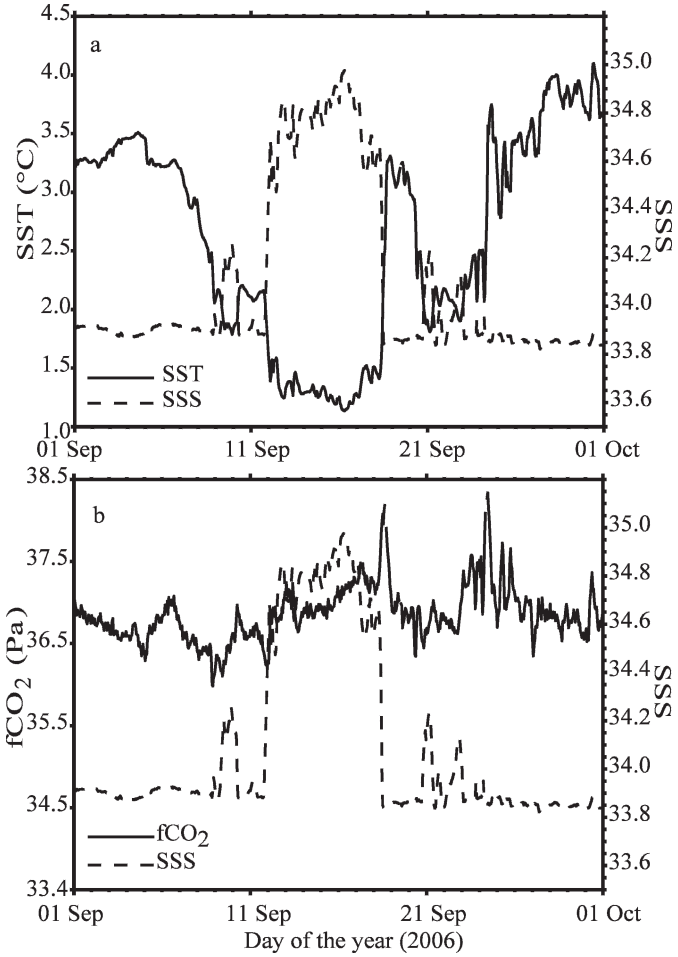

Fig. 14. Measurements of buoy No. 9 from 01 Sep to 01 Oct 2006. (a) SSS and SST, and (b) SSS and fCO_2. Temperature and salinity suggest that CARIOCA No. 9 sampled an episodic event of LCDW outcropping at the ocean surface over a few days. The event has no signature in fCO_2.

~1.0 Pa lower than atmospheric value; in the PZ, CARIOCA ΔfCO_2 averages −0.6 Pa. They observe a seasonal variation of DIC in 40°S–50°S of ~30 μmol kg^{-1} between winter and summer months (with maxima in winter) but almost no seasonal variation in fCO_2 because of compensation between increasing DIC and decreasing SST in winter. Similarly, from CARIOCA observations we estimate a seasonal variation of 29 μmol kg^{-1} between Feb–Mar and Aug.

Interpreting measurements from quasi-Lagrangian drifters is quite challenging because it does not follow exactly surface currents, and we show that localizing measurements precisely with respect to Southern Ocean fronts greatly helps the interpretation of fCO_2 and DIC measurements. Future work using ship measurements should benefit from the methodology we propose for locating in situ surface measurements with respect to the location of fronts. We found that the detection of the SAF from SST gradients, as proposed by Moore et al. (1999), worked well in the mid–Atlantic Ocean, as was already found by Burls and Reason (2006), but was ambiguous when applied across all the longitudes of the Southern Ocean because the SST range in

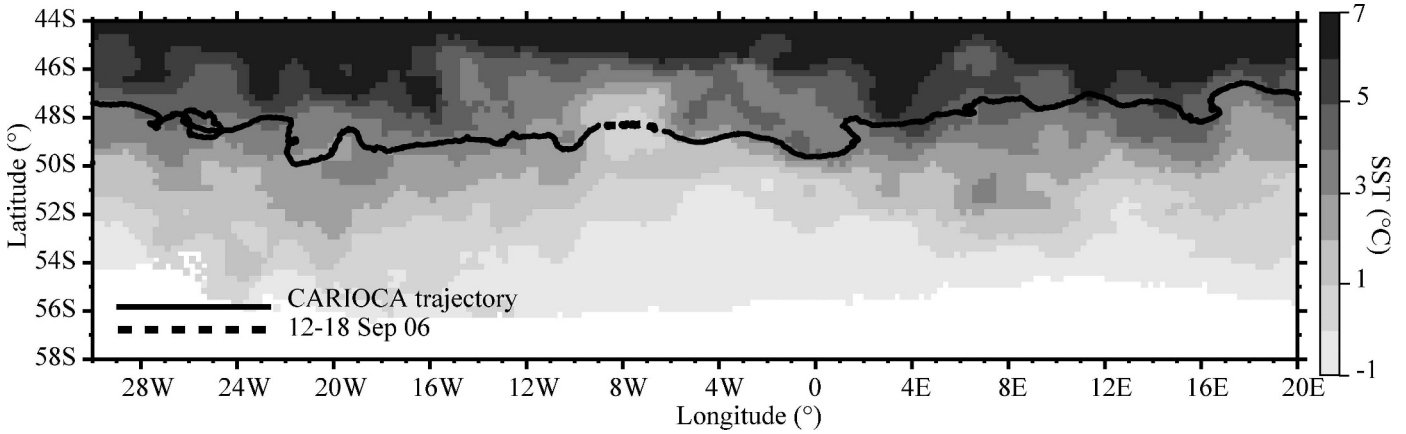

Fig. 15. AMSRE SST on 15 Sep 2006, when the buoy No. 9 measured a low SST and high SSS anomaly. CARIOCA trajectory is shown as a solid line, with the 12 to 18 Sep 2006 period shown as a dashed line.

which the gradient detection has to be done varies with longitude; in addition this SST range seems to vary seasonally. On the other hand, we found that the detection of fronts using sea-surface height derived from altimetry clearly identifies the area where fCO_2 is measured.

In addition to large-scale seasonal variability, standard deviations of fCO_2 measured by a CARIOCA drifter within a single season range from 0.6 Pa to 1.6 Pa. In order to understand the source of this variability, some sections of CARIOCA trajectories have been studied in detail.

In the southern Indian Ocean, the mixing of different water masses close to the SAF and STF and warming in the SAZ are responsible for >2.0 Pa variability of fCO_2 on a small scale (<50 km).

It is known that close to the subtropical front, submesoscale lateral density structures are created in the oceanic-surface mixed layer (Hosegood et al. 2006). In addition, density-compensated layers have already been observed in eddies and subduction zones close to the STF (Boyer De Montégut 2005). CARIOCA measurements show that in these areas strong DIC variations (about 10 μmol kg^{-1}) associated with strong fCO_2 variations (about 2.0 Pa) occur on a kilometric scale, suggesting that large DIC values are likely to come from the deep layer at the base of the compensated layers; given that this observation was made at the onset of winter, high DIC in the compensated layer might result from the remineralization of biological material produced in the surface layer during previous seasons.

These observations highlight the need for high-resolution measurements for describing and understanding mesoscale variability of surface carbon parameters.

Close to the PF, CARIOCA sampled an episodic event of LCDW outcropping at the ocean surface over a few days. It is remarkable that although this event has a strong signature in SSS and SST anomalies, no fCO_2 anomaly is visible due to compensation between high DIC and low SST and SSS.

References

Aoki, S., M. Hariyama, H. Mitsudera, H. Sasaki, and Y. Sasai. 2007. Formation regions of subantarctic mode water detected by OFES and Argo profiling floats Geophys. Res. Lett. **34:** L10606, doi:10.1029/2007GL029828.

Baker, D., and others. 2006. TransCom 3 inversion intercomparison: Impact of transport model errors on the interannual variability of regional CO_2 fluxes, 1988–2003 Glob. Biogeochem. Cycles **20:** GB1002, doi:10.1029/2004GB002439.

Bakker, D. C. E., J. Etcheto, J. Boutin, and L. Merlivat. 2001. Variability of surface-water fCO_2 during seasonal upwelling in the equatorial Atlantic Ocean as observed by a drifting buoy J. Geophys. Res. **106:** 9241–9254.

Bates, N. R., L. Merlivat, L. Beaumont, and C. Pequignet. 2000. Intercomparison of shipboard and moored CARIOCA buoy seawater measurements in the Sargasso Sea Mar. Chem. **72:** 239–255.

Belkin, I. M., and A. L. Gordon. 1996. Southern ocean fronts from the Greenwich meridian to Tasmania J. Geophys. Res. **101:** 3675–3696.

Boutin, J., and J. Etcheto. 1997. Long term variability of the air–sea CO_2 exchange coefficient: Consequences for the CO_2 fluxes in the equatorial Pacific Ocean Glob. Biogeochem. Cycles **11:** 453–470.

———, J. Etcheto, L. Merlivat, and Y. Rangama. 2002. Influence of gas exchange coefficient parameterization on seasonal and regional variability of CO_2 air–sea fluxes Geophys. Res. Lett. **29:** 1182, doi:10.1029/2001GL013872, 2002.

Boyer de Montégut, C. 2005. Couche mélangée océanique et bilan thermohalin de surface dans l'océan Indien Nord. Ph.D. thesis. Univ. of Paris.

Breviere, E., N. Metzl, A. Poisson, and B. Tilbrook. 2006. Changes of the oceanic CO_2 sink in the Eastern Indian sector of the Southern Ocean Tellus **58B:** 436–448.

Burling, R. W. 1961. Hydrology of circumpolar waters south of New Zealand N. Z. Dep. Sci. Ind. Res. Bull. **143**.

Burls, N. J., and C. J. C. Reason. 2006. Sea surface temperature fronts in the midlatitude South Atlantic revealed by using microwave satellite data J. Geophys. Res. **111:** C08001, doi:10.01029/2005JC003133.

Chierici, M., A. Fransson, D. R. Turner, E. A. Pakhomov, and P. W. Froneman. 2004. Variability in pH, fCO_2, oxygen and flux of CO_2 in the surface water along a transect in the Atlantic sector of the Southern Ocean Deep Sea Res. II **51:** 2773–2787.

Copin-Montégut, C., M. Bégovic, and L. Merlivat. 2004. Variability of the partial pressure of CO_2 on diel to annual time scales in the northwestern Mediterranean Sea Mar. Chem. **85:** 169–189.

Dafner, E., and others. 2003. Major nutrients and dissolved oxygen as indicators of the frontal zones in the Atlantic sector of the Southern Ocean J. Geophys. Res. **108:** 3227, doi:10.1029/1999JC000288.

Deacon, G. E. R. 1982. Physical and biological zonation in the Southern Ocean Deep Sea Res. **29:** 1–15.

Dong, S., J. Sprintall, and S. Gille. 2006. Location of the polar front from AMSR-E satellite sea surface temperature measurements J. Phys. Oceanog. **36:** 2075–2089.

Emery, W. J., and R. E. Thomson. 1997. Data analysis methods in physical oceanography. Gray.

Gille, S. T., D. P. Stevens, R. T. Tokmakian, and K. J. Heywood. 2001. Antarctic circumpolar current response to zonally-averaged winds J. Geophys. Res. **106:** 2743–2759.

Gloor, M., N. Gruber, J. Sarmiento, C. L. Sabine, R. A. Feely, and C. Rodenbeck. 2003. A first estimate of present and preindustrial air–sea CO_2 flux patterns based on ocean interior carbon measurements and models Geophys. Res. Lett. **30:** 1010, doi:10.1029/2002GL015594.

Ho, D. T., C. S. Law, M. J. Smith, P. Schlosser, M. Harvey, and P. Hill. 2006. Measurements of air–sea gas exchange at high wind speeds in the Southern Ocean: Implications for global parameterizations Geophys. Res. Lett. **33:** L16611, doi:10.1029/2006GL026817.

Hood, E. M., and L. Merlivat. 2001. Annual to interannual variations of fCO_2 in the northwestern Mediterranean Sea: High frequency time series data from CARIOCA buoys (1995–1997) J. Mar. Res. **59:** 113–131.

Hosegood, P., M. C. Gregg, and M. H. Alford. 2006. Sub-mesoscale lateral density structure in the oceanic surface mixed layer Geophys. Res. Lett. **33:** L22604, doi:10.1029/2006GL026797.

Hughes, C. W., M. Meredith, and K. Heywood. 1999. Wind driven transport fluctuations through Drake Passage: A southern mode J. Phys. Oceanog. **29:** 1971–1992.

Lee, K., and others. 2006. Global relationships of total alkalinity with salinity and temperature in surface waters of the world's oceans Geophys. Res. Lett. **33:** L19605, doi:10.1029/2006GL027207.

Lefèvre, N., J. P. Ciabrini, G. Michard, B. Brient, M. Duchaffaut, and L. Merlivat. 1993. A new optical sensor for P_{CO2} measurements in sea water Mar. Chem. **42:** 189–198.

Lequéré, C., and others. 2007. Saturation of the Southern ocean CO_2 sink due to recent climate change Science **316:** 1735–1738, doi:10.1126/science.1136188.

Lueker, T. J., A. G. Dickson, and C. D. Keeling. 2000. Ocean pCO_2 calculated from dissolved inorganic carbon, alkalinity, and equations for K1 and K2: Validation based on laboratory measurements of CO_2 in gas and seawater at equilibrium Mar. Chem. **70:** 105–119.

McNeil, B. I., N. Metzl, R. M. Key, and R. J. Matear. 2007. An empirical estimate of the Southern Ocean air–sea CO_2 flux Glob. Biogeochem. Cycles **21:** GB3011, doi:10.1029/2007GB002991.

Metzl, N., C. Brunet, A. Jabaud-Jan, A. Poisson, and B. Schauer. 2006. Summer and winter air–sea CO_2 fluxes in the Southern Ocean Deep Sea Res. I **53:** 1548–1563.

———, N. B. Tilbrook, and A. Poisson. 1999. The annual fCO_2 cycle and the air–sea CO_2 flux in the sub-Antarctic Ocean Tellus **51B:** 849–861.

Millero, F. J., T. B. Graham, F. Huang, H. Bustos-Serrano, and D. Pierrot. 2006. Dissociation constants of carbonic acid in seawater as a function of salinity and temperature Mar. Chem. **100:** 80–94.

Moore, J. K., M. R. Abott, and J. G. Richman. 1999. Location and dynamics of the Antarctic polar front from satellite sea surface temperature data J. Geophys. Res. **104:** 3059–3073.

Naegler, T., P. Ciais, K. B. Rodgers, and I. Levin. 2006. Excess radiocarbon constraints on air–sea gas exchange and the uptake of CO_2 by the oceans Geophys. Res. Lett. **33:** L11802, doi:10.1029/2005GL025408.

Niiler, P. P., N. A. Maximenko, and J. C. McWilliams. 2003. Dynamically balanced absolute sea level of the global ocean derived from near-surface velocity observations Geophys. Res. Lett. **30:** 2164, doi:10.1029/2003GL018628.

Olbers, D., D. Borowski, C. Volker, and J.-O. Wolf. 2004. The dynamical balance, transport and circulation of the Antarctic Circumpolar Current Antarct. Sci. **16:** 439–470, doi:10.1017/S0954102004002251.

Orsi, A. H., and T. Whitworth. 2005–2006. Hydrographic atlas of the world ocean experiment (WOCE). Volume 1: Southern Ocean. International WOCE project office.

———, ———, and W. D. Nowlin. 1995. On the meridional extent and fronts of the Antarctic circumpolar current Deep Sea Res. I **42:** 641–673.

Patra, P. K., S. Maksyutov, M. Ishizawa, T. Nakazawa, T. Takahashi, and J. Ukita. 2005. Interannual and decadal changes in the sea–air CO_2 flux from atmospheric CO_2 inverse modelling Glob. Biogeochem. Cycles **19:** GB4013, doi:10.1029/2004GB002257.

Sallée, J., R. Morrow, and K. Speer. 2008*a*. Eddy heat diffusion and Subantarctic mode water formation Geophys. Res. Lett. **35:** L05607, doi:10.1029/2007GL032827.

———, K. Speer, and R. Morrow. 2008*b*. Response of the Antarctic circumpolar current to atmospheric variability J. Clim. **21:** 3020–3039.

Steele, L. P., P. B. Krummel, and R. L. Langenfelds. 2002. Atmospheric CO_2 concentrations from sites in the CSIRO Atmospheric Research GASLAB air sampling network, p. #. *In* EDITOR(S) [ed.], Trends: A compendium of data on global change (Oct 2002 version). U.S. Department of Energy, Oak Ridge National Laboratory, Carbon Dioxide Information Analysis Center.

Sweeney, C., E. Gloor, A. R. Jacobson, R. M. Key, G. McKinley, J. L. Sarmiento, and R. Wanninkhof. 2007. Constraining global air–sea gas exchange for CO_2 with recent bomb ^{14}C measurements Glob. Biogeochem. Cycles **21:** GB2015, doi:10.1029/2006GB002784.

Takahashi, T., and others. 2002. Global sea–air CO_2 flux based on climatological surface ocean pCO_2 and seasonal biological and temperature effects Deep Sea Res. II **49:** 1601–1622.

———, and others. In press. Climatological mean and decadal change in surface ocean pCO_2, and net set-air CO_2 flux over the global oceans. Deep-Sea Res. II.

Wanninkhof, R. 1992. Relationship between wind speed and gas exchange over the ocean J. Geophys. Res. **97:** 7373–7382.

———, and others. 2006. Carbon dioxide, hydrographic, and chemical data obtained during the R/V *Ronald H. Brown* repeat hydrography cruise in the Atlantic Ocean: CLIVAR CO_2 Section A16S_2005 (11 Jan–24 Feb 2005). *In* A. Kozyr [ed.], ORNL/CDIAC-151, NDP-087. U.S. Department of Energy, Oak Ridge National Laboratory, Carbon Dioxide Information Analysis Center.

Weiss, R. F. 1974. Carbon dioxide in water and seawater: The solubility of a nonideal gas Mar. Chem. **2:** 203–215.

Zeebe, R. E., and D. W. Gladrow. 2001. CO_2 in seawater: Equilibrium, kinetics, isotopes. Elsevier Oceanography Series.

Received: 2 October 2007
Accepted: 7 April 2008
Amended: 30 June 2008